Step-width Adjustment and Sidewall Control in Electron-beam Lithography

by

Pengcheng Li

A thesis submitted to the Graduate Faculty of
Auburn University
in partial fulfillment of the
requirements for the Degree of
Master of Science

Auburn, Alabama
December 13, 2010

Keywords: proximity effect correction, dose control, step-width adjustment, sidewall control

Approved by

Soo-Young Lee, Professor of Electrical and Computer Engineering
Stanley J. Reeves, Professor of Electrical and Computer Engineering
Bogdan M. Wilamowski, Professor of Electrical and Computer Engineering

Abstract

Two-dimensional (2-D) patterns and three-dimensional (3-D) structures increasingly find applications in various devices such as diffractive optical elements, photonic element, microelectromechanical systems (MEMS) etc. and are often fabricated by e-beam lithography. Their performance is known to be highly sensitive to their dimensions. Therefore, it is critical to achieve high dimensional accuracy for the desired characteristics. However, as the feature size decreases down to nanoscale, the non-ideal exposure distribution due to electron scattering can make dimensions of the fabricated features in a device substantially different from the target dimensions. In this thesis, the issue of controlling the dimensions of the features transferred onto the resist layer is addressed for the staircase structures and the line patterns. The remaining resist profile estimated from the 3-D exposure distribution is employed in the optimization procedure in order to obtain realistic results. The results from the experiments and extensive simulation study are analyzed.

Acknowledgments

I would like to thank my advisor Dr. Soo-Young Lee for all his support, detailed guidance and helpful suggestions throughout the entire development of PYRAMID for three-dimensional lithography without which this thesis would not have been possible. I would also like to thank the other members of my committee, Dr. Stanley J. Reeves and Dr. Bogdan M. Wilamowski for their support and help. Thanks are also due to the National NanoFab Center for experiment and characterization services, and Samsung Electronics Co. for funding this research, and to Auburn University and Department of ECE for their financial support. Also, I would like to thank Mr. Qing Dai for helping me get familiar with the PYRAMID programs. Last but not least, I would like to thank my family, my friends and all other people who have given me help during my MS study.

To my loved family members and heavenly abodes, without whose support I would not be able to be where I am now.

Table of Contents

List of Figures

List of Tables

Chapter 1

Introduction

Miniaturization and performance improvements are the central concerns in modern fabrication technology, and electron-beam (e-beam) lithography is one of the key technologies to fabricate devices at nanometer scale due to its very short wavelength [1]. Two-dimensional and three-dimensional patterns are transferred onto a resist layer via e-beam lithographic process in various applications, e.g., discrete devices [2], photomasks [3], molds for imprint lithography [4], etc. However, proximity effect (or non-ideal exposure distribution) due to the forward and backward-scattering of electrons results in undesirable blurring of the transferred pattern. The degree of proximity effect mainly depends on the beam accelerating voltage, resist thickness, substrate material and beam diameter [5].

As the feature size is reduced well below a micron and the circuit density continues to increase, the relative variation of feature dimensions, due to the proximity effect, becomes larger. Hence, it is crucial to have a practical scheme to minimize the dimensional deviation from the target pattern. In most schemes, an empirical approach which relies on the experimentally determined relationship between the e-beam dose or exposure and remaining resist thickness is taken. However, such an approach takes into account neither the resist development process nor possible variation of feature size, thus possibly resulting in substantial dimensional errors $[6-9]$. Therefore, in order to have an accurate control of the remaining resist profile, an analytic model which considers the resist development processes, in addition to the exposure distribution, is required. In this study, such a model is employed for step-width adjustment in staircase structures and controlling sidewall shape in line patterns.

1.1 Previous Work

Numerous researches on proximity effect correction and the related issues have been conducted by many researchers for many years [10 − 20]. The fundamental difficulties in proximity effect correction are the large size of data involved and the constraint of non-negative solution (dose). The two critical issues are the accuracy and speed of correction. Most of the correction schemes adopted either dose or shape modification to achieve a desirable exposure distribution. In general, the accuracy and complexity of a correction scheme depend on the model which describes the e-beam lithographic process, in addition to the correction scheme itself. Many models ignore the forward-scattering of electrons and the exposure variation along the depth dimension of resist.

PYRAMID [21 − 35], a hierarchical rule-based approach toward proximity effect correction, was introduced for fast and accurate correction. It has been demonstrated that PYRAMID can handle the feature size of nanoscale. Its correction hierarchy is flexible such that various correction models can be implemented. The PYRAMID implementations include the shape modification [27], the dose modification [36], the heterogeneous substrate correction [37], the grayscale correction [38], the non-rectangular feature correction [39], etc.. More recently, the PYRAMID was further developed by employing a 3-D model where the exposure variation along the depth dimension is considered. The difference between the 2-D and 3-D models, in terms of their effects on correction results, was analyzed [40]. Correction based on the 3-D model was considered for discrete-level grayscale structures and binary patterns. In particular, controlling the step depth in staircase structures was investigated via simulation and experiment [41]. Also, controllability of the sidewall shape in line patterns was studied through simulation [42].

1.2 Motivation and Objectives

It was noticed in the fabrication of discrete-level structures such as a staircase that the actual step-width can be substantially deviated from the target width. Therefore, it is necessary to control the width as well as the height of each step. Also, in the case of line pattern, a different sidewall shape of line may be preferred in a different application. Hence,

it is desirable to have a certain degree of control over the sidewall shape. The problem of sidewall control can be viewed as a generalization of the step-width control in a discrete-level structure where the number of levels (steps) is large. The objectives of this study are to develop a step-width adjustment scheme and further refine the sidewall control scheme based on the recent results from the PYRAMID project.

1.3 Organization of the Thesis

This thesis is organized as follows:

• Chapter 2 introduces the algorithms for estimating remaining resist profile based on the 3-D exposure model.

• Chapter 3 describes the step-width adjustment scheme for staircase structures, which employs both dose and shape modifications.

• Chapter 4 includes the results from analyzing the relationship among the total dose, spatial distribution of dose, developing time and sidewall shape, and implementing the SA (simulated annealing) for dose optimization

• Chapter 5 presents conclusions and suggestions for the future work.

Chapter 2

Estimation of Remaining Resist Profile

In this chapter, the 3-D model of exposure distribution (therefore rate distribution) and resist development simulation are briefly reviewed [47], following an introduction of e-beam lithography.

2.1 Electron Beam Lithography

E-beam lithography is the process of transferring the circuit patterns from photo lithographic mask to the resist using a focused beam of electrons. The primary advantage of e-beam lithography is that it offers high patterning resolution and versatile pattern formation. Thus e-beam lithography is the most commonly used technique for nanolithography.

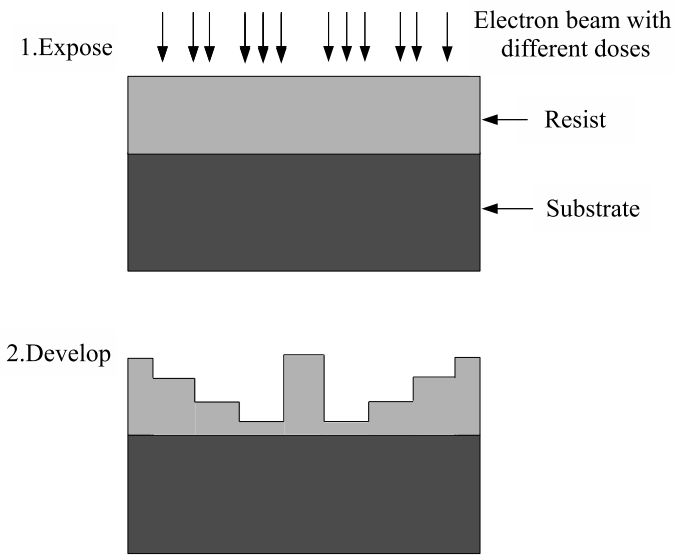

Figure 2.1: Illustration of the e-beam grayscale lithographic process.

As illustrated in Figure 2.1, a resist is exposed by e-beam, depositing energy in the resist, and the amount of energy at each location depends on how electrons are scattered.

Then a solvent developer is used to selectively remove either exposed (positive photoresist) or unexposed regions (negative photoresist). For the positive photoresist, the resist is removed where the energy deposited is higher than a certain threshold exposure value. After development process, the remaining resist profile serves as a mask to selectively etch the substrate material, transferring the circuit patterns onto the substrate if necessary.

2.2 Point Spread Function

For high-quality proximity effect correction and estimation of resist profile, the accurate knowledge of *point spread function* (PSF) is required in e-beam lithography. A PSF shows how the electron energy is distributed throughout the resist when a single point is exposed. As shown in Figure 2.2 (a), the PSF is a function of the distance from the exposed point and radically symmetric in three dimensions. In general, the PSF depends on the resist thickness, beam energy, beam diameter, substrate composition, etc., and is independent on the dose given to the point. For homogeneous substrate, the PSF does not vary with the position of the point exposed.

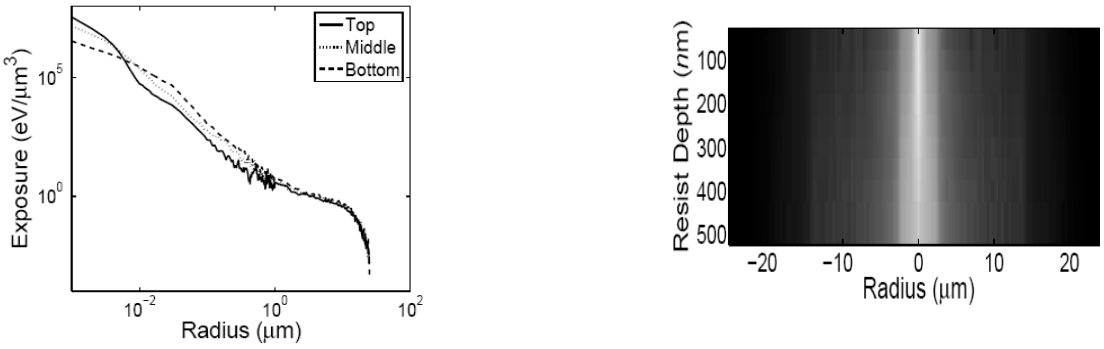

(a) (b)

Figure 2.2: A PSF for the substrate system of 500 nm PMMA on Si with the beam energy of 50 KeV : (a) the top, middle and bottom layers, and (b) all layers

Theoretical modeling such as a double-Gaussian function or a Monte Carlo simulation $[43-44]$ is used to get the PSF. It can be seen from Figure 2.2 (a) and (b) that a PSF

can be decomposed into two components, the *local* component due to electron's forward-scattering and the *global* component due to electron's backward-scattering. Within the local component, the PSF has large magnitude and is very sharp, but it varies rapidly. While the magnitude of the global component is orders of magnitude lower than that in the forward-scattering range and varies slowly.

2.3 3-D Exposure Model

E-beam lithographic process can be assumed to be linear and space invariant for uniform substrates. Therefore, the exposure deposited in the resist can be estimated by the convolution between the circuit pattern (dose distribution) and a PSF. In 3-D exposure model, a 3-D PSF is used, and thus the depth-dependent proximity effect is considered.

Consider an X-Y plane which corresponds to the top surface of the resist layer, as shown in Figure 2.3 (a). Let $d(x, y, 0)$, $e(x, y, z)$, and $psf(x, y, z)$ represent the e-beam dose to the point $(x, y, 0)$ at the surface of the resist, the exposure at the point (x, y, z) in the resist, and the PSF, respectively. Then the 3-D exposure distribution can be computed as follows:

$$e(x, y, z) = \int\int d(x - x', y - y', 0) psf(x', y', z) dx' dy' \tag{2.1}$$

In this study, exposure is computed by an accurate and efficient two-level procedure implemented in the PYRAMID software [24] which is decomposed into *local* exposure and *global* exposure. Local exposure is the exposure contributed by the features close to the exposed point under consideration and global exposure is the sum of exposure contributions by features far away from the point at which exposure is calculated. When the circuit pattern is sufficiently long (in the Y-dimension in Figure 2.3 (a)), exposure can be assumed not to vary along the Y-dimension in most of the structure. In such a case, consideration of only a cross section in the middle of the pattern shown in Figure 2.3 (b) is sufficient. Hence, in the remainder of this thesis, the Y-dimension is not taken into account, i.e., only the cross section in the X-Z plane will be considered.

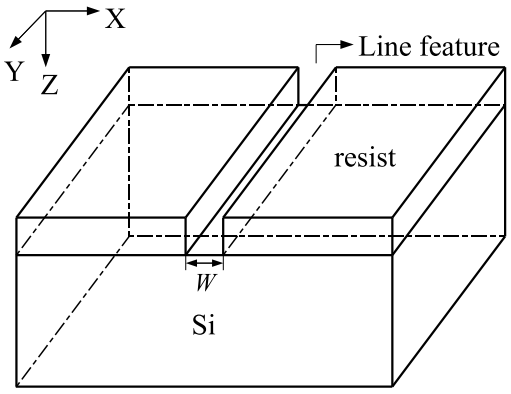

(a)

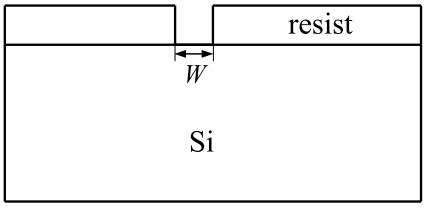

(b)

Figure 2.3: (a) A line pattern transferred onto resist and (b) the cross section of the remaining resist profile.

Though the 3-D exposure model estimates how electron energy is distributed throughout the resist, it does not depict the remaining resist profile explicitly after development. Therefore, the resist development process simulation should be taken into account for proximity effect correction in order to get more realistic and accurate correction results.

2.4 Developing Rate

To simulate the remaining resist profile after development, the resist developing rate matrix $r(x, z)$ (nm/min) at point (x, z) is transformed from the exposure matrix $e(x, z)$ (eV/μm^3). The relationship between exposure and resist developing rate is known to be nonlinear [46]. For high accuracy of proximity effect correction, the relationship has been derived from the experimental results. The exposure-to-rate conversion formula depends on developing time and the resist-solvent combination. As exposure increases, developing rate increases more than linearly, i.e., the increase is slow in the beginning and then faster. But, when exposure exceeds a certain value, developing rate tends to saturate (though this region is not utilized in this study). Such behavior of developing rate may be modeled by a curve or a part of curve with an inflection point, including the 3rd polynomial and Gaussian curves.

2.5 Width Variation

The width of a feature such as a single line or each step of a staircase structure may vary along the resist depth as illustrated in Figure 2.4. Let $W(z)$, W_t, W_m, and W_b denote the width of the feature which is a function of resist depth z, the widths of a feature at the top, middle and bottom layers of the resist, respectively. Note that $W_t > W_m > W_b$ and $W_t < W_m < W_b$ indicate overcut and undercut sidewalls, thus the order of feature width $W(z)$ specifies the type of sidewall. Due to the lateral development of the resist and spatial distribution of dose, the actual feature width deviates from the target one, even causing the sidewall shape to be changed. For example, the actual resist profile is overcut, though the desired one is undercut or vertical sidewall. Therefore, the proximity effect correction method is carried out to minimize the deviation between the actual and target widths of a feature.

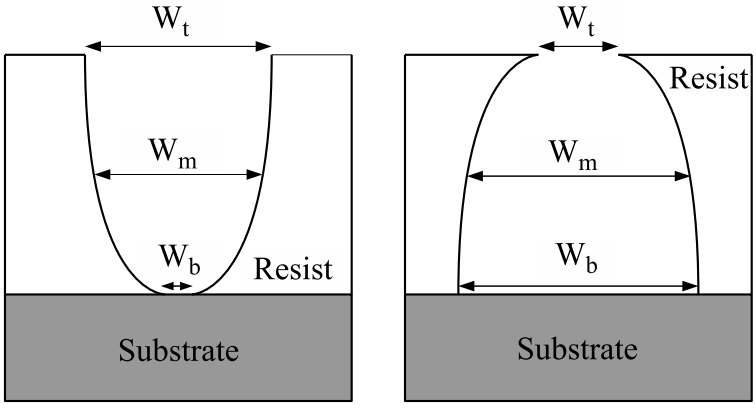

Figure 2.4: Cross section of the remaining resist for a line feature: (a) overcut and (b) undercut

2.6 Resist Development Algorithm

With the advancement of MEMS fabrication techniques and the increasing complexity of IC design, accurate and efficient simulation processes such as resist development, are greatly needed, in order to reduce development cost and fabrication experiments. One of the difficulties in resist development simulation is the resist development algorithm. Several kinds of algorithms have been proposed: the ray tracing algorithm, the string algorithm, and the cell removal algorithm. The former two algorithms sometimes causes fatal errors such as looping of rays or strings. While the cell removal algorithm is absolutely stable and robust [47] but it costs considerably computational time. Also, the method to estimate the resist profile depends on the patterns under consideration.

2.6.1 Resist Development Algorithm of Discrete-level Structures

For discrete-level structures, such as staircase structures in Figure 3.1(a), one way to estimate the resist profile is to rely on a full-scale resist development simulation such as the cell removal method which is too time-consuming to be practical especially in an iterative procedure. Also, for step-width adjustment, only step-widths, rather than a complete resist profile, need to be estimated. A practical and yet sufficiently accurate method has been

developed for step-width estimation. Using $e(x, z)$ obtained by simulation and the final conversion formula, $r(x, z)$ is computed. The slope of step-edge is also affected by the proximity effect and is not usually vertical. However, for simplicity, the width of a step is measured at the middle level between two adjacent steps, as illustrated in Figure 2.5. For each step in the staircase, the time duration, Δt_i , during which the second half of the final step-height is developed, is derived based on $r(x, z)$ (refer to Figure 2.5). Then the location of the step-edge in the developed resist profile is estimated by computing the amount of lateral development during Δt_i, from which the step-width deviation is obtained. The deviation of step-edge with respect to the target location is denoted by ΔW_i, as illustrated in Figure 2.6, and the deviation of step-width compared to the target width is represented by $\epsilon_{Wi} = |\Delta W_i - \Delta W_{i+1}|$ for $i = 1$, 2, 3, and 4 ($2\Delta W_i$ for $i = 5$). Finally, the actual step-width W_i' of step i can be calculated by $W_i' = W_i \pm \epsilon_{Wi}$ where W_i is the target step-width of step i. Figure 2.7 is one application of resist profile estimation using the proposed method for discrete-level structures, thus this method is developed to adjust step-width of staircase structures.

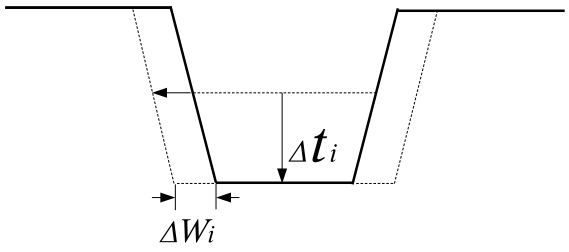

Figure 2.5: Estimation of step-edge deviation where Δt_i is the time taken for the half of the step-height to be developed.

2.6.2 Resist Development Algorithm of Continuous Structures

For continuous features, such as the line pattern, the full-scale resist development algorithm is still required to depict the resist profile. A simplified version of the resist development process model, PEACE [47], is employed to estimate the remaining resist profile after

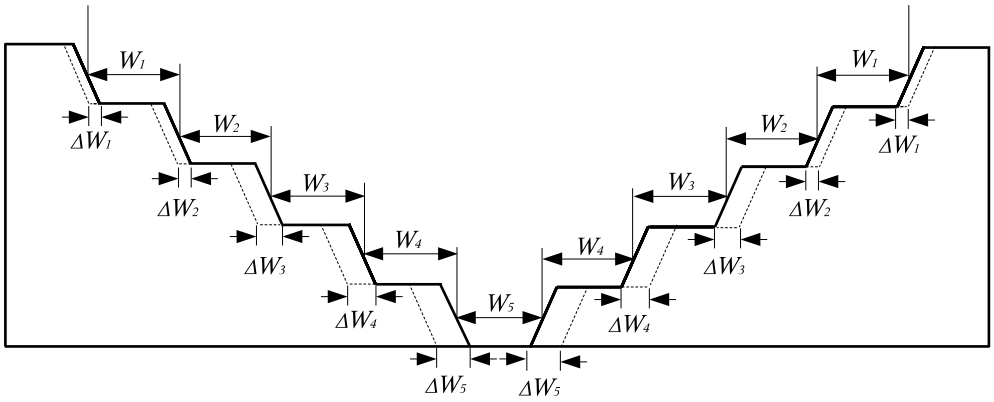

Figure 2.6: Step-edge deviations in a staircase structure

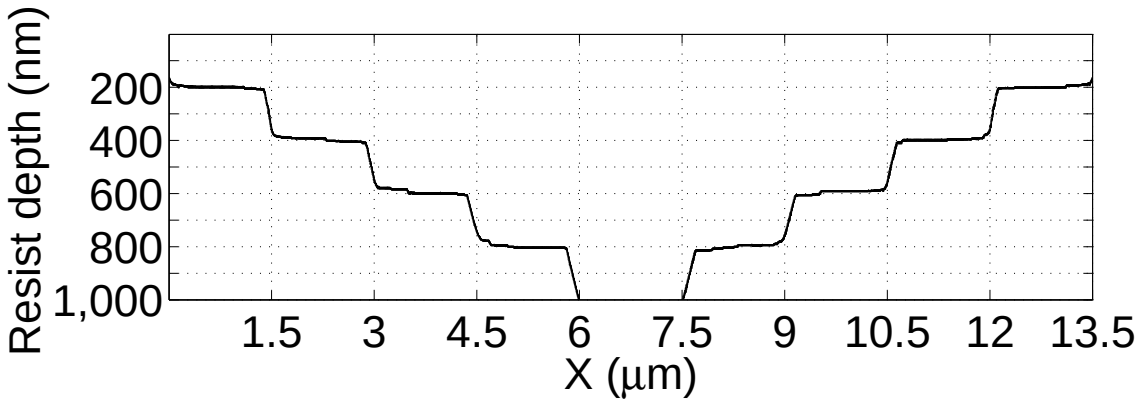

Figure 2.7: The remaining resist profile of discrete-level structure.

development. The cell removal method is based on time evolution of the resist front, and the amount of each cell to be etched in each step depends on the minimum dissolution time dT and its neighboring cells in contact with the developer. The dT, the minimum dissolution time to fully develop a cell in the current surface front, is computed and then the status of other cells are updated for the elapsed time dT. When a cell is removed, its neighboring cells start to be developed. Note that the dT is estimated from not only the cell under consideration, but also its neighbors. By tracking and updating the status of all cells, the cell removal method is able to simulate the resist development process. Thus, the cells are removed in the order that the development proceeds.

The computationally-intensive nature of the cell removal method makes the proximity effect correction procedure extremely time-consuming since the development simulation

needs to be carried out many times through iterations. Also, it often results in rough resist profiles. With the assumption that a feature varies only in one dimension such as a long line, a new simulation method was recently developed in our group, which is orders of magnitude faster than the cell removal method and generates smooth profiles. The overall shapes of profiles obtained by the new method are equivalent to the respective profiles by the cell removal method. It first considers only vertical development and subsequently all possible developing paths consisting of lateral development following vertical development. The resist profiles obtained by the cell removal and new method are shown in Figure 2.8.

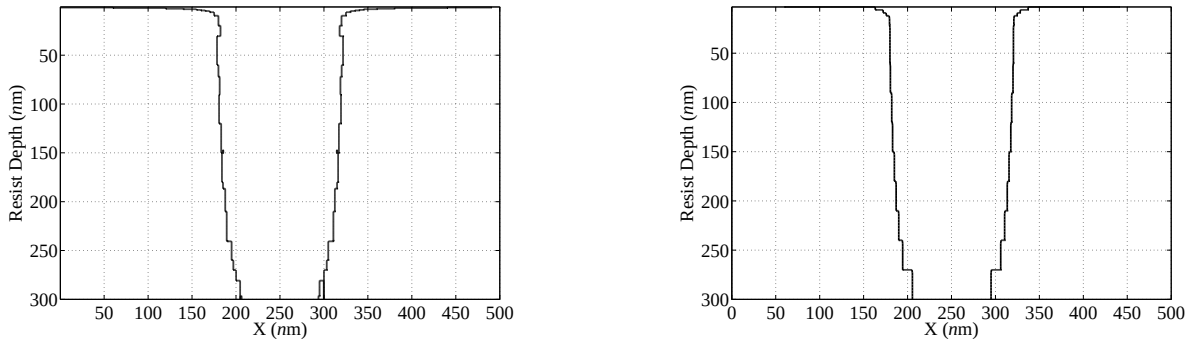

(a) (b)

Figure 2.8: The remaining resist profile of a line pattern estimated from (a) cell removal and (b) new method.

Chapter 3

Adjustment of Step-Width

The issue of improving the dimensional accuracy of 3-D structures fabricated by e-beam grayscale lithography is addressed for structures with discrete levels. Specifically, a step-width adjustment scheme is developed for accurately controlling the (remaining) resist profiles of staircase structures. The goal of the scheme is to minimize the step-width error in the resist profile. The scheme is based on 3-D exposure and resist development models [41]. An exposure-to-developing rate conversion formula is derived based on experimental results. Then, a resist development scheme with the rate conversion formula is employed to estimate the resist profile from which the amount of adjustment in step-width is determined. Performance of the step-width adjustment scheme has been analyzed through computer simulation and also experiments. It has been shown that this practical scheme is effective in reducing the step-width error.

3.1 Model

In Figure 3.1(a), a symmetric nine-step staircase structure is illustrated and the cross section in the middle of the staircase is shown in Figure 3.1(b). As shown in Figure 3.1(b), step i refers to the ith step from the left.

3.1.1 Derivation of Developing Rate

Let the relationship be represented by a non-linear function $F[\ ]$ to be referred to as (exposure-to-developing rate) *conversion formula*. Then, $r(x, z)$ is given by $r(x, z) = F[e(x, z)]$. Let $p(x)$ denote the resist profile, i.e, the depth measured from the initial surface of the resist downward as shown in Figure 3.1(b). When the step-width is wide, the developing process at the center of the step progresses mainly in the vertical direction such that the lateral development may be ignored. Then, for the center of each step, the depth $p(x)$ can

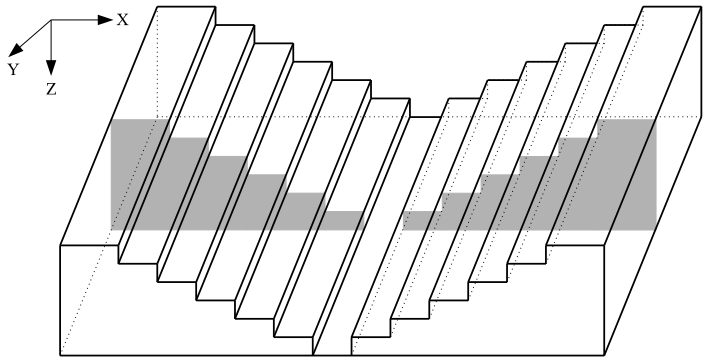

(a)

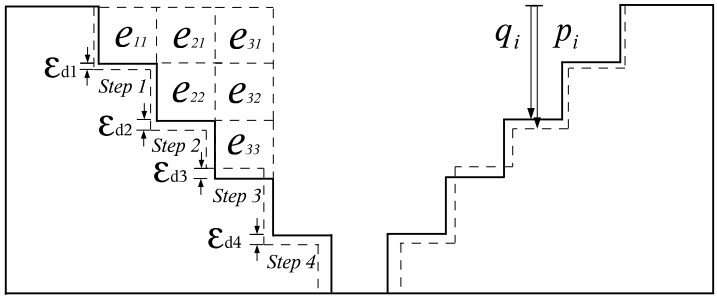

(b)

Figure 3.1: (a) A nine-step staircase structure and (b) its cross section where the solid and dashed lines are target and actual profiles, respectively.

be related to the developing rate in the contiguous domain, as in Equation 3.1 where T is the developing time.

$$\int_0^{p(x)} \frac{dz}{r(x,z)} = T \tag{3.1}$$

In the experimental result of a staircase structure, only the discrete depth information is available, i.e., one depth for each step (refer to Table 3.1). Let p_i denote the depth of step i measured at the center of the step in an experimental result and q_i the target depth of step i. The depth error of step i is represented by $\epsilon_{di} = |p_i - q_i|$. Also, the cross section is partitioned into blocks, as shown in Figure 3.1(b). Exposure is considered to be homogeneous within each block and e_{ij} denotes the exposure in the jth block of step i.

Developer	Step	Dose (μC/cm^2)	Exposure (eV/μm^3)	Depth p_i (nm)
MIBK:IBA = 1:1	1	216	1.7286×10^{10}	182
	2	296	2.0983×10^{10}	417
	3	334	2.2489×10^{10}	626
	4	364	2.3751×10^{10}	852
	5	396	2.5229×10^{10}	1000

Table 3.1: Experimental result for a nine-step symmetric staircase structure fabricated on 1000 nm PMMA on Si (50 KeV): dose, exposure, and depth.

Derivation of the exposure-to-rate conversion formula is carried out in two phases. In the first phase, the depth-dependent exposure or rate variation is not considered by using the average value of e_{ij} for each step, which is denoted by e_i. Accordingly, the average developing rate r_i for each step is defined. From experiments, p_i is obtained and r_i is estimated to be $\frac{p_i}{T}$ for step i. Then, the set of sample points, $\{e_i, r_i\}$, is fitted to a curve to derive the conversion formula. The behavior of developing rate may be modeled by a Gaussian curve. As shown in Figure 3.2, a part of the left half of a Gaussian function $r_i = a \times exp(-(\frac{e_i - b}{c})^2)$ is employed in order to minimize the number of coefficients to be determined in curve fitting. Note that a third-order polynomial involves four coefficients. One problem of the first phase is that it does not take the depth-dependent exposure (and therefore rate) variation into account, which would cause a significant error in estimating depth and width of a step.

In the second phase, the conversion formula obtained in the first phase is used as an initial solution for an iterative refining procedure. In each iteration, the block-wise exposure distribution e_{ij} is used to estimate the depth of step i, to be denoted by p'_i, based on the current conversion formula. Then, the coefficients a, b, and c, in the conversion formula are adjusted such that the error $\sum |p_i - p'_i|$ is minimized through an exhaustive search. From several sets of experimental data, the following conversion formula was obtained:

$$r(x,z) = 4024.2 \times e^{-(\frac{e(x,z) \ -3.4 \ \times \ 10^{10}}{1.0968 \ \times \ 10^{10}})^2} \tag{3.2}$$

where $e(x,z)$ is in eV/μm^3 and $r(x,z)$ is in nm/min.

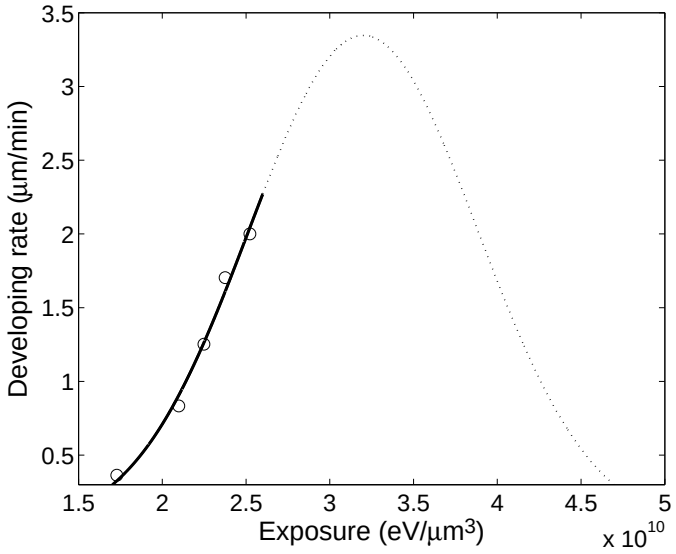

Figure 3.2: Exposure-developing rate curve for MIBK:IPA = 1:1 (lines with symbols) with developing time of 30 *sec*. The circles are experimental data to which a part of Gaussian curve is fitted.

The average percent error in curve fitting is 4.41% and the range of exposure used in the adjustment scheme is from 0 to 3.4×10^{10} eV/μm^3.

3.2 Estimation of Step-Width Deviation

Due to the isotropic process of resist development, the vertical wall between adjacent steps in a staircase structure is developed laterally, causing the step-width to be different from the target width. In Figure 3.4(a), a simulated resist profile of staircase structure is provided where it can be seen that the deviation of center step-width is as large as 16%. For step-width adjustment, the step-width deviation first needs to be estimated as described in Section 2.6. It should be noted that in the case of the staircase structure considered in this study, step-width adjustment is equivalent to step-edge adjustment.

3.3 Step-Width Adjustment

A practical scheme for adjusting step-widths has been developed that minimizes the computational requirement by avoiding a complete resist development simulation. As shown in Figure 3.3, the scheme proceeds as follows.

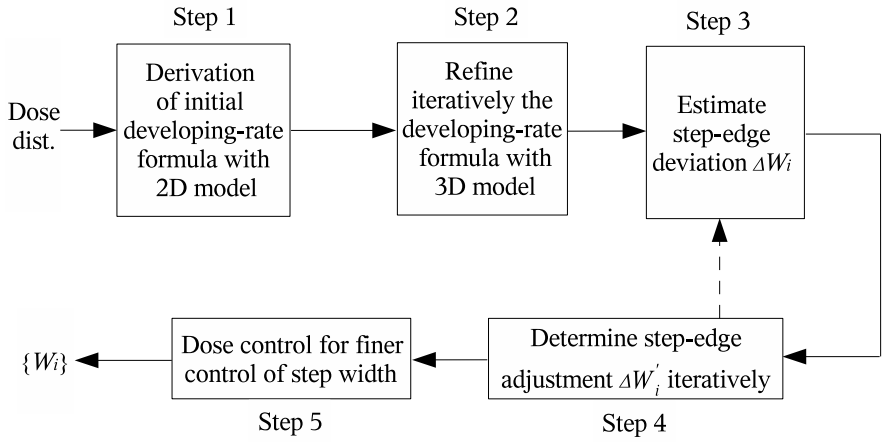

Figure 3.3: Step-width adjustment scheme

Step 1: The 2-D exposure distribution is computed by the PYRAMID software[24] and the initial developing rate formula is derived, based on the experimental result (depth of each step).

Step 2: The conversion formula is refined iteratively, using the 3-D exposure distribution computed by the PYRAMID software (refer to Section 2.3).

Step 3: The step-edge deviation, ΔW_i, is estimated for each step, given a developing time, using the method described in Section 2.6.

Step 4: The amount of step-edge adjustment, $\Delta W_i'$, to compensate for ΔW_i, is determined through an iterative procedure. In each iteration, the edge location (equivalent width) of each step (step i) is adjusted by ΔW_i before recomputing the exposure distribution from which ΔW_i is estimated, as in Step 3. This is repeated until the adjustment of the edge location in an iteration is less than a half of pixel. The final step-edge locations (or widths) obtained through the iterative procedure are further adjusted to compensate for the minor overestimation by simulation, i.e., $\Delta W_i' \leftarrow c \times dW_i$, where dW_i is the difference between the initial and final step-edge locations and the c is a constant less than 1.

Step 5: In many cases, one may not achieve the target widths with high precision due to the fact that the step-width can be adjusted only by whole pixels. Also, an adjustment of step-width also changes the exposure distribution, especially in the neighboring areas. Hence, in order to have finer control in adjusting step-width and also to compensate for the exposure change due to step-width adjustment, the dose adjustment may be carried out along with the width adjustment. The dose adjustment is carried out by the grayscale PYRAMID software [41].

3.4 Results and Discussion

3.4.1 Simulation Results

The 3-D test structure used in this study is a symmetric staircase structure consisting of nine steps where the width and length of each step are 1.5 μm and 50 μm, respectively. The substrate system is composed of 1000 nm poly (methyl methacrylate) (PMMA) on Si and the beam energy is assumed to be 50 KeV .

In Figures 3.4(a) and (b), the resist profiles obtained without and with width adjustment are provided along with the step-edge (ΔW_i) and width (ϵ_{Wi}) deviations in the figure caption. Note that in order to show the detail, the vertical (depth) dimension is scaled up (relative to the horizontal dimension). It can be seen that the resist profile before width adjustment shows a significant edge deviation of each step and a larger deviation for a deeper step. The reason why the center step has the largest width error (deviation) is that the directions of lateral development on the left and right edges of the center step are opposite. Therefore, the step-width deviation (ϵ_{Wi}) for the center step is twice the step-edge deviation (ΔW_i) in this symmetric staircase. However, for other steps, the step-edge deviations at the left and right edges are in the same direction. Hence, the step-width deviation of a step is smaller than the step-edge deviation of either edge. Also, the higher exposure at the center step helps to make ΔW_i larger than those for other steps. The final profile after step-width adjustment, combined with the dose control scheme in Figure 3.4(b), is significantly closer to the target profile and shows a substantial improvement in step-width accuracy.

In Figure 3.5, the simulation results for a symmetric staircase structure with a smaller step-width of 1 μm and a thinner resist of 500 nm are provided. It is observed that the step-edge and width deviations are smaller than those for the thicker resist of 1000 nm since the developing time is shorter, i.e., less time for lateral development. Again, through step-width adjustment, a resist profile much closer to the target profile has been obtained. Note that the cell removal model is carried out to simulate the remaining resist profile of staircase structures only and also to verify the accuracy of the step-width adjustment scheme, and it is not used for the step-width deviation estimation.

3.4.2 Experimental Results

The symmetric nine-step staircase structure with the step-width of 1.5 μm adopted in the simulation study has been fabricated with and without step-width adjustment. The substrate system was prepared by spin-coating a Si wafer with 1000 nm PMMA and soft-baked at 160 ^oC for 1 minute. The structure was written using an Elionix ELS-7000 e-beam

tool with acceleration voltage of 50 KeV and beam current of 100 pA. The sample was developed in MIBK:IPA = 1:1 for 30 seconds. The remaining resist was coated with 10 nm Pt before the cross section was imaged by a FEI FE-SEM (Sirion). For easier inspection of the cross section, the length of the structure was increased to 500 μm. The SEM images of the cross section are provided in Figure 3.6.

It is seen in Figure 3.6(a) that the width of the center step is 11.3% wider than the target width. As mentioned in Section 2.6, the width deviation for the center step was estimated to be 16% in the simulation, which is reasonably close to the experimental result. As shown in Figure 3.6(b), the step-width adjustment not only reduced the width deviation greatly, but also decreased the step-height deviation, ϵ_{di}, making the step-height closer to the target height of 200 nm. In Figure 3.7, the step-width deviations measured in the simulation and experimental results, before and after step-width adjustment, are plotted. In the experimental result, the maximum step-width deviation was reduced from 170 nm down to 10 nm and the average step-width deviation was from 37.8 nm to 2.2 nm where the target width is 1.5 μm. Also, the simulation result closely agrees with the experimental result, which well demonstrates the accuracy of our simulation model and step-width adjustment scheme.

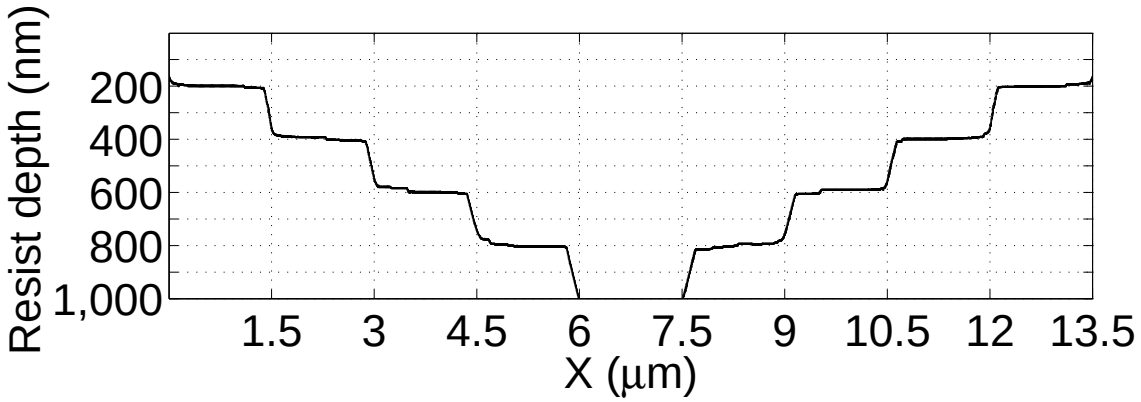

(a)

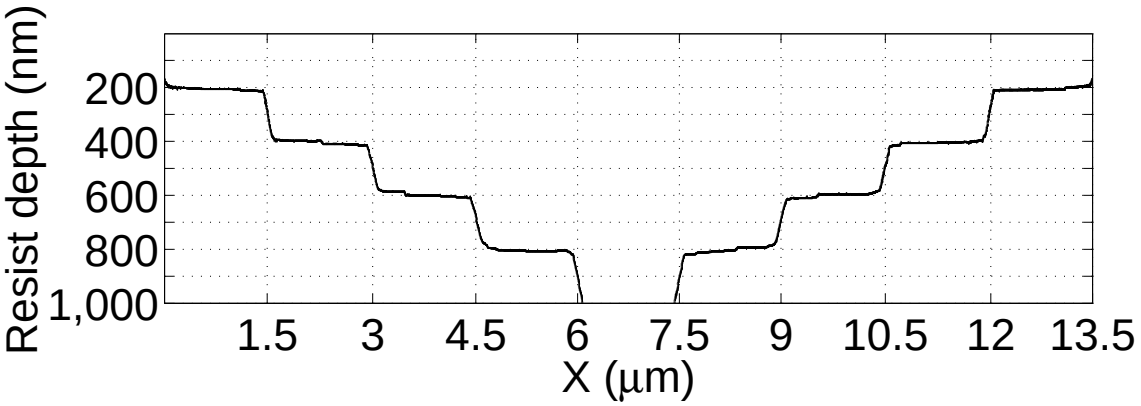

(b)

Figure 3.4: (a) Step-edge deviation: $\{\Delta W_i\} = \{0, 45, 70, 90, 125, 125, 90, 70, 45, 0\ n\text{m}\}$ Step-width deviation: $\{\epsilon_{Wi}\} = \{45, 25, 20, 35, 250, 35, 20, 25, 45\ n\text{m}\}$ (b) Step-edge deviation: $\{\Delta W_i\} = \{0, 0, 0, 0, 0, 0, 0, 0, 0, 0\ n\text{m}\}$ Step-width deviation: $\{\epsilon_{Wi}\} = \{0, 0, 0, 0, 0, 0, 0, 0, 0\ n\text{m}\}$ Remaining resist profiles obtained (through simulation) for the staircase structure (a) before adjustment and (b) after step-width and dose adjustments where target step-width: 1.5 μm, target step-height: 200 nm, resist thickness: 1000 nm on Si (50 KeV). A deviation less than 1 nm is rounded to zero.

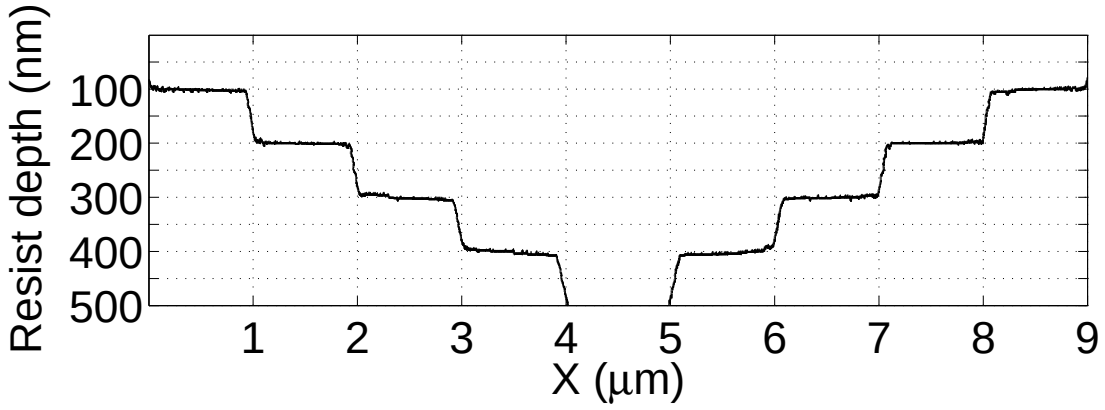

(a)

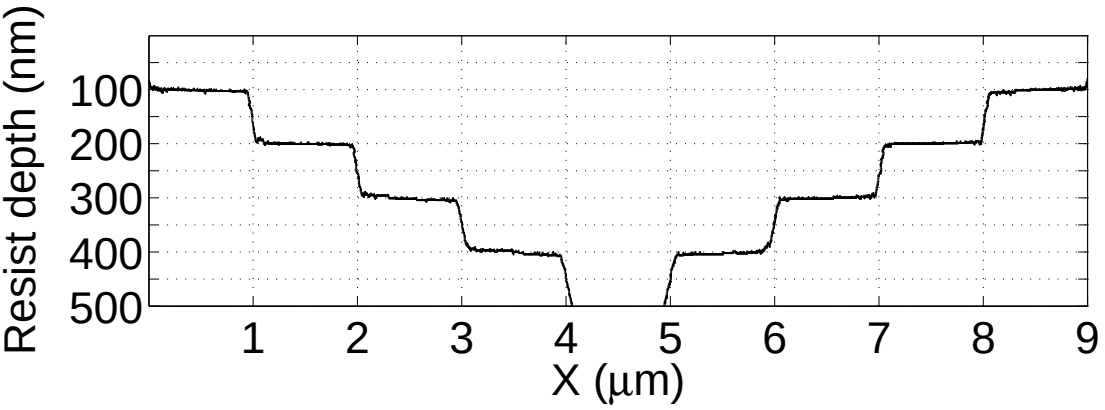

(b)

Figure 3.5: (a) Step-edge deviation: $\{\Delta W_i\} = \{0,\ 15,\ 25,\ 35,\ 60,\ 60,\ 35,\ 25,\ 15,\ 0\ n\text{m}\}$ Step-width deviation: $\{\epsilon_{Wi}\} = \{15,\ 10,\ 10,\ 25,\ 120,\ 25,\ 10,\ 10,\ 15\ n\text{m}\}$ (b) Step-edge deviation: $\{\Delta W_i\} = \{0,\ 0,\ 0,\ 0,\ 0,\ 0,\ 0,\ 0,\ 0,\ 0\ n\text{m}\}$ Step-width deviation: $\{\epsilon_{Wi}\} = \{0,\ 0,\ 0,\ 0,\ 0,\ 0,\ 0,\ 0,\ 0\ n\text{m}\}$ Remaining resist profiles obtained (through simulation) for the staircase structure (a) before adjustment and (b) after step-width and dose adjustments where target step-width: 1.0 μm, target step-height: 100 nm, resist thickness: 500 nm on Si (50 KeV). A deviation less than 1 nm is rounded to zero.

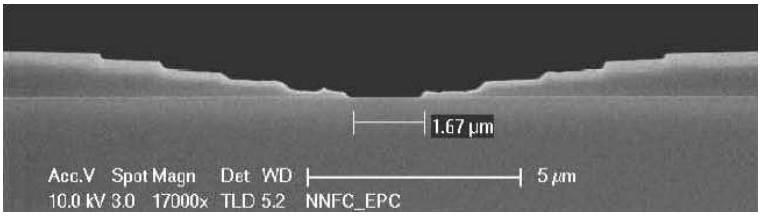

(a)

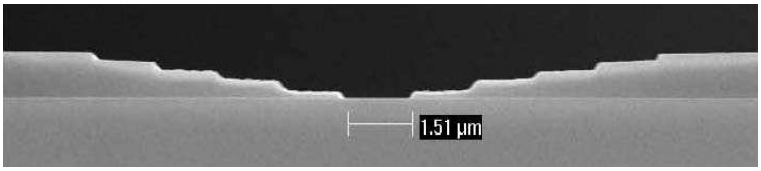

(b)

Figure 3.6: Experimental results (a) before step-width adjustment and (b) after step-width adjustment where target step-width: 1.5 μm, target step-height: 200 nm, resist thickness: 1000 nm PMMA on Si (50 KeV).

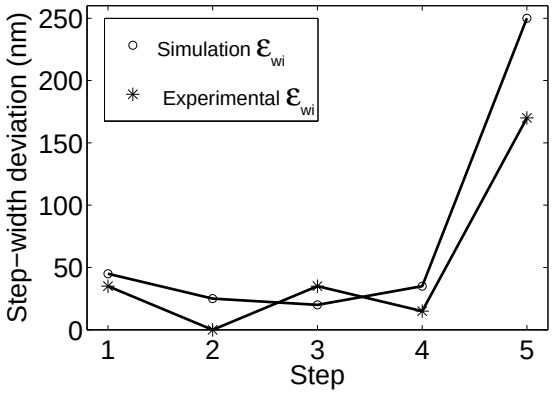

(a)

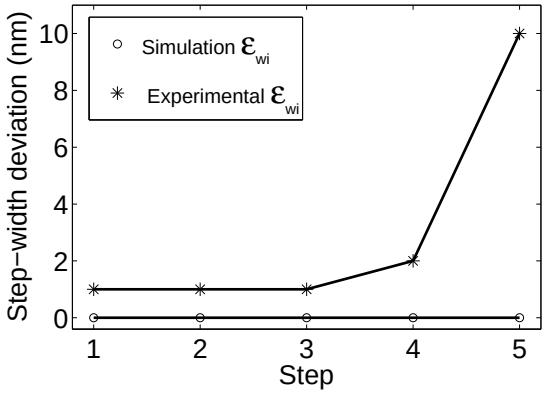

(b)

Figure 3.7: Step-width deviations in simulation and experimental results (a) before step-width adjustment and (b) after step-width adjustment for 1000 nm PMMA (50 KeV).

Chapter 4

Controlling Sidewall of Resist Profile

A certain type of resist profile is desired depending on the subsequent process following resist development [6]. For example, an undercut profile is required for lift-off and a straight vertical sidewall for etching. As the feature size is reduced down to nanoscale, the aspect ratio of developed feature in the resist profile becomes larger even for a thin resist. This makes a small variation in the sidewall slope cause a relatively large critical-dimension (CD) error. Therefore, it is important to have a sufficient control over the sidewall shape in the resist profile. The sidewall shape obtained through e-beam lithographic process depends on factors such as exposure (energy deposited in resist) distribution, developing time, etc. Varying developing time is a passive approach in that the spatial exposure distribution is set, and therefore has a limited controllability. Controlling the exposure distribution, more precisely the 3-D distribution of exposure, enables a more explicit method to achieve a target sidewall. Nevertheless, in most of the previous work, only the dose level was varied with a uniform dose within a feature, to achieve different shapes of sidewall, and the 3-D exposure distribution was not considered. Changing the level of uniform dose only scales the exposure distribution without altering the spatial distribution and therefore does not fully utilize the available controllability of exposure distribution [42]. Here, a general-purpose optimization method, Simulated Annealing (SA), is adopted in determining the dose distribution required for target sidewall shapes.

4.1 3-D Model

The sidewall of resist profile for a line pattern is considered as illustrated in Figure 2.3(a) and its cross section plane (X-Z plane) is shown in Figure 2.3(b).

4.1.1 Developing Rate

The developer and developing time used to fabricate the single line are MIBK:IBA = 1:2 and 40 *sec*, respectively, which are different from those in fabrication of staircase structures, thus the exposure-to-rate conversion formula needs to be re-derived. At the center of a line (in the cross section plane) where the exposure is highest when a uniform dose is given to the line, resist development progresses mainly downward (i.e., along the vertical dimension) such that the lateral development may be ignored. Exploiting this property, the conversion formula is derived using a part of the 3rd-order polynomial curve. It models the cross section of resist layer by a 2-D array of blocks within each of which the exposure and therefore developing rate are assumed to be constant. Using the remaining resist profile from experiments, the conversion formula is calibrated iteratively by modeling the developing rate block by block of the vertical column at the center of the line.

The following conversion formula was obtained:

$$r = 2.8 \times 10^{-29} \times e^3 + 4.9 \times 10^{-19} \times e^2 + 0.39 \times 10^{-8} \times e \tag{4.1}$$

where e is in eV/μm^3 and r is in nm/min.

4.1.2 Simulation of Resist Development

For the sidewall shape control, the fast and accurate resist development simulation mentioned in Section 2.6.2 is employed to find the optimal dose distribution to achieve the target sidewall shape because of its high efficiency. When a small region has a much higher exposure than its surrounding regions, its effective developing rate is significantly lower than the nominal rate (given by Eqn. 4.1 due to the aspect-ratio-dependent development). To reflect this effect in development simulation, the developing rate is adjusted according to the spatial distribution of exposure before the simulation.

4.2 Sidewall Control

Given a developer and a developing time, the resist profile depends on the exposure distribution $e(x, z)$. Therefore, one may attempt to control $e(x, z)$ in order to achieve a target

resist profile. When a substrate system is given, $e(x, z)$ is determined by the distribution of e-beam dose within the feature, i.e., a line. The e-beam dose is varied (controlled) only along the width dimension, i.e., X-axis and therefore the dose distribution is denoted by $d(x)$. The feature considered in this study is a long line and the cross section of resist profile at the center of the line is characterized by the line widths in the top, middle and bottom layers as illustrated in Figure 4.1. Let rx_i and px_i represent the target and actual widths in the ith layer, respectively. Then, the optimization problem for sidewall control can be defined as finding $d(x)$ such that the cost function $max_i(|rx_i - px_i|)$ is minimized.

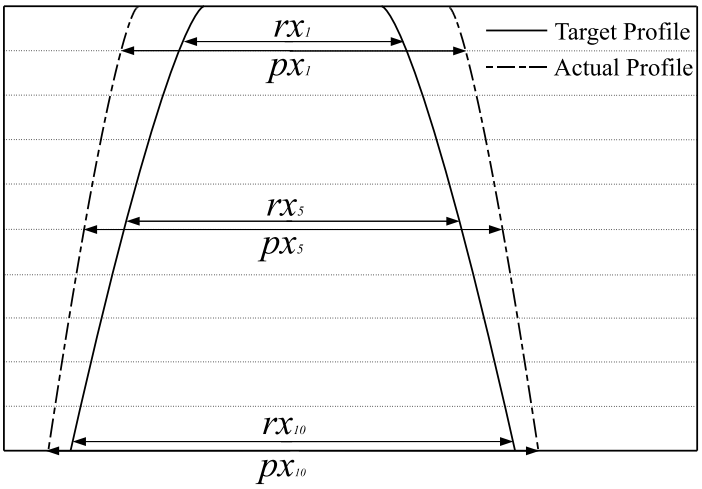

Figure 4.1: An illustration of sidewall shape specification in the cross section: rx_i and px_i are the target and actual widths of line in the ith layer of resist, respectively. The cost function is defined as $C = max_i(|rx_i - px_i|)$.

In order to avoid an impractically long computation time, the line is partitioned into n regions along the length dimension as shown in Figure 4.2(b) and a dose for each region is to be determined. That is, the solution from the optimization is a dose set $(d_1, d_2, \cdots, d_n)$ where d_j is the dose for the jth region. A fundamental difficulty of this optimization is that the optimal dose for a region has conflicts among layers, i.e., the dose required for a layer may be different from that for another layer. Also, the optimal dose for a region depends on the doses of the other regions. In this study, the general-purpose optimization method of

Simulated Annealing (SA) is adopted, which perturbs the doses of multiple regions in each iteration to find a globally optimal solution [49].

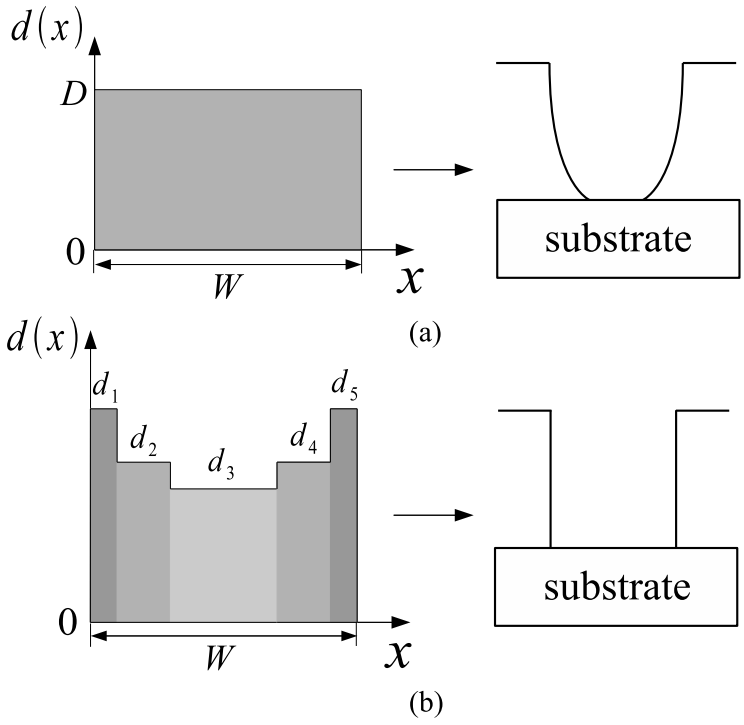

Figure 4.2: Dose distribution and the corresponding sidewall shape: (a) a uniform dose distribution and (b) the spatially-controlled dose distribution.

A single dose for all regions, minimizing the cost function, is first determined as an initial solution. For evaluation of the cost function, the exposure distribution in the cross section is computed through the convolution between the dose distribution and the point spread function. Then, the resist development simulation is carried out to measure the dimensional errors in terms of line widths, i.e., $|rx_i - px_i|$. The main optimization procedure of SA starts from the initial solution and iteratively derives the optimal or an acceptable solution. The flowchart of SA is given in Figure 4.3 and the steps in SA are described below. The solution obtained in the kth iteration is denoted by $S'^{(k)} = (d_1^{(k)}, d_2^{(k)}, ..., d_i^{(k)}, ..., d_n^{(k)})$ where $d_i^{(k)}$ is the dose for the ith region, derived in the kth iteration.

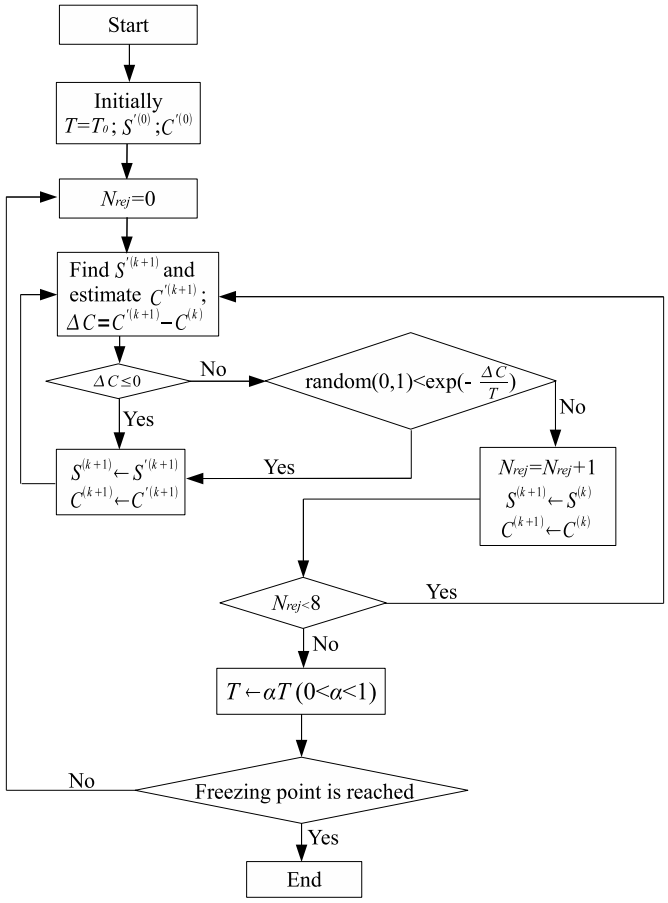

Figure 4.3: The flowchart of SA (simulated annealing) process

Step 1: Initially, the solution S is set to $S'^{(0)}=(d_1^{(0)}, d_2^{(0)}, ..., d_i^{(0)}, ..., d_n^{(0)})$, and the temperature T to a high value of T_0. A possible initial dose distribution is a uniform distribution, i.e., $d_i^{(0)} = d_j^{(0)}$ for all i, j. The cost function $C = max_i(|rx_i - px_i|)$ is evaluated based on $S'^{(0)}$ through resist development simulation. Let $C'^{(0)}$ denote the value of the cost function for $S'^{(0)}$.

Step 2: Randomly perturb the current solution (spatial dose distribution) $S^{(k)}$ to a potential new solution $S'^{(k+1)} = S^{(k)}+(\Delta d_1^{(k+1)}, ..., \Delta d_i^{(k+1)}, ..., \Delta d_n^{(k+1)})$, where $S^{(k)}$ is the accepted dose distribution in the kth iteration and $\Delta d_i^{(k+1)}$ is the amount of dose change for the ith region in the $(k+1)$th iteration. Note that the doses of all regions are adjusted as illustrated in Figure 4.4. In the case of single line, the dose distribution

must be symmetric with respect to the center of line. Therefore, only $\frac{n+1}{2}$ $\Delta d_i^{(k+1)}$'s need to be determined. Determination of $\Delta d_i^{(k+1)}$ may be guided by a certain heuristic. In this study, $\Delta d_i^{(k+1)}$ is computed as follows

$$\Delta d_i^{(k+1)} = \left(0.5 \times (d_{max} - d_{min} - d_{minJump}) \times (1 + \cos(\frac{j \times \pi}{J})) + d_{minJump}\right) \times (r - 0.5) \tag{4.2}$$

where d_{max} and d_{min} are the upper and lower limits of dose allowed, $d_{minJump}$ is the minimum dose step of $\Delta d_i^{(k+1)}$, j is the index for the jth temperature decrement from T_0 to the current T, J is the total number of temperature decrements and r is a random number ranging $[0, 1]$.

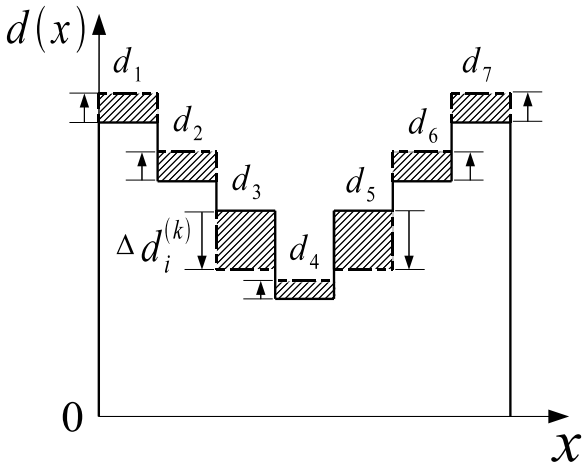

Figure 4.4: During the SA process, the doses of all regions of a line feature are adjusted. The solid line and dashed lines represent the dose distribution before and after dose adjustment.

Note that the dose step range is adjusted (decreased) as the temperature is decreased as shown in Figure 4.5. The cost function C is evaluated for $S'^{(k+1)}$ to obtain its cost $C'^{(k+1)}$.

Step 3: When $\Delta C = C'^{(k+1)} - C^{(k)} < 0$ where $C^{(k)}$ is the value of cost function for $S^{(k)}$, $S'^{(k+1)}$ is accepted to become $S^{(k+1)}$. If $\Delta C > 0$, $S'^{(k+1)}$ is still accepted with the probability

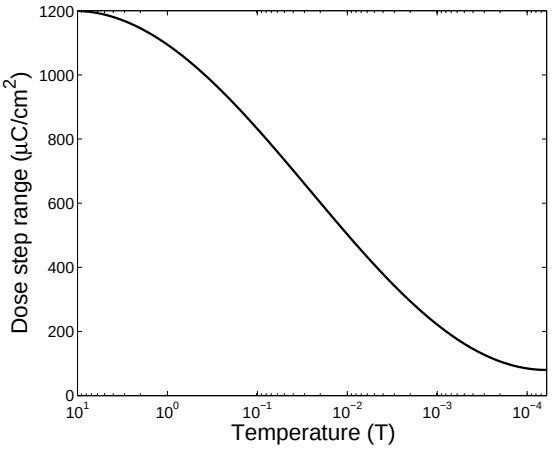

Figure 4.5: Dose step range vs temperature in the SA process.

of $exp(-\frac{\Delta C}{T})$. This acceptance of a worse solution enables the hill-climbing capability of SA toward the globally optimal solution. Otherwise, $S'^{(k+1)}$ is rejected in which case $S^{(k)}$ becomes $S^{(k+1)}$. If the number of successive rejections N_{rej} exceeds a certain threshold, go to Step 4. Otherwise, go to Step 2.

Step 4: The temperature T is lowered according to $T \leftarrow \alpha \times T$ where $0 < \alpha < 1$. That is, as the SA progresses, a worse solution is accepted less (since it is likely that the current solution is closer to the optimal solution). Go to Step 2 if T is above the final temperature. Otherwise, go to Step 5.

Step 5: The current solution is taken as the final solution (dose distribution).

Constraints

The optimization of the dose distribution may be done with or without constraints such as total dose, developing time, etc. It is always desirable to minimize the time to expose a pattern from the viewpoint of throughput. The exposing time is mainly proportional to the total dose to be given to the pattern. Also, the smaller the total dose is, the lower the charging effect is. Hence, a dose distribution of which the total dose is smaller is better as long as it achieves an equivalent quality of the resist profile. In most of our study, the constraint of the same total (average) dose was imposed, i.e., $DW = \int_0^W d(x)dx$ where D is a certain dose level and W is the line width as shown in Figure 4.2. In other words, the same

total dose is redistributed over the line (feature) through optimization in order to achieve a certain target profile.

4.3 Results and Discussion

Three different dose distributions were considered in computer simulation as shown in Figure 4.6. One, referred to as *Distribution-A*, is a uniform distribution. Another, referred to as *Distribution-B*, is the one where the edge dose is moderately larger than the center dose. The other, referred to as *Distribution-C*, has the edge dose much larger than the center dose.

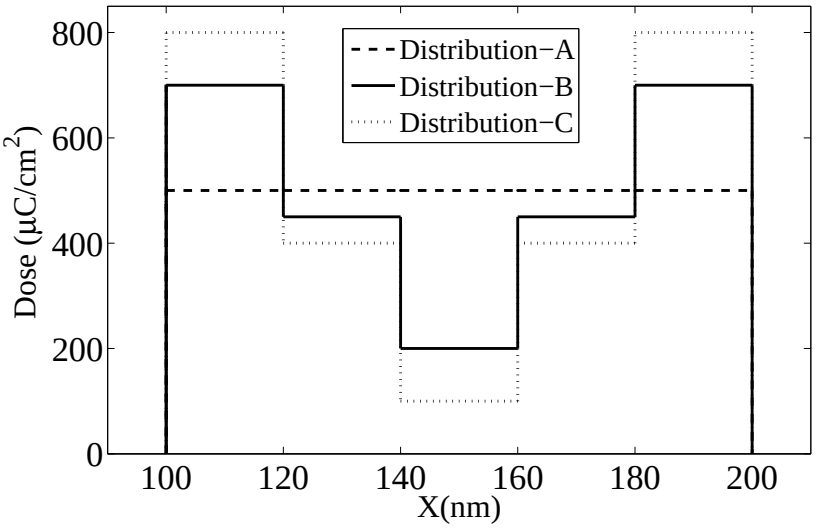

Figure 4.6: Three dose distributions of *Distribution-A*, *Distribution-B* and *Distribution-C*

4.3.1 Simulation Results

The test feature used in this study is a single line where the width and length of the line are 100 nm and 50 μm, respectively. The substrate system is composed of 300 nm PMMA on Si and the beam energy is assumed to be 50 KeV. The total (or average) dose is fixed in each set of results unless specified otherwise.

The relationship among the dose distribution, total dose, and developing time in terms of their effects on the sidewall shape has been analyzed through simulation. The sidewall shapes obtained for the three different dose distributions (Figure 4.6) with the total dose and developing time fixed are shown in Figure 4.7 and the line-width measurements are provided in Table 4.1. It can be seen that a different dose distribution leads to a different sidewall shape. For a vertical sidewall, the Distribution-B minimizes the width error (among the three). The developing time required for a target sidewall shape ($rx_1 = 130n$m, $rx_5 = 130n$m, $rx_{10} = 130n$m) was derived for each of the dose distributions in Figure 4.6. The Distribution-B requires the shortest developing time to achieve the sidewall shape closest to the target one (refer to Table 4.2). The three dose distributions were scaled by a certain factor to achieve the target sidewall shape and the results are provided in Table 4.3. The Distribution-B requires the lowest total (average) dose while minimizing the width error.

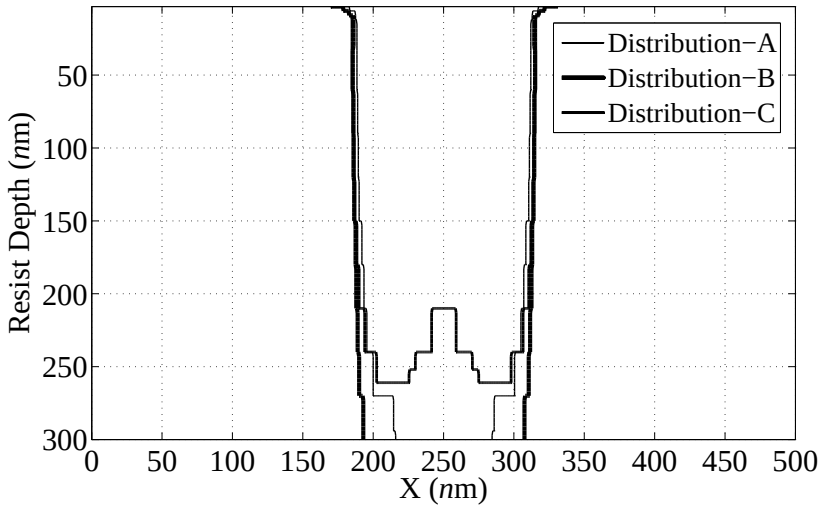

Figure 4.7: The remaining resist profiles (sidewall shapes) of *Distribution-A*, *Distribution-B* and *Distribution-C*.

In Figure 4.8, the remaining resist profiles obtained from the three different types of spatial dose distributions are provided for the average dose of 500 $\mu C/cm^2$. The target sidewall shape is vertical. When the dose is not controlled, i.e., a constant dose of 500

Dose Distribution	Average Dose ($\mu C/cm^2$)	Developing Time (sec)	Resist Profile (nm) Line Width		
			px_1	px_5	px_{10}
A:Dashed curve	500.0	40.0	124.4	117.0	71.4
B:Solid curve	500.0	40.0	129.8	126.0	115.0
C:Dotted curve	500.0	40.0	131.4	124.0	0.0

Table 4.1: Effects of the dose distribution on the sidewall shape with the total (average) dose and developing time fixed.

Dose Distribution	Average Dose ($\mu C/cm^2$)	Developing Time (sec)	Resist Profile (nm) Line Width		
			px_1	px_5	px_{10}
A:Dashed curve	500.0	66.0	131.7	131.0	129.0
B:Solid curve	500.0	51.0	133.0	132.0	129.0
C:Dotted curve	500.0	60.0	137.5	135.0	128.0

Table 4.2: The developing time required to achieve the same (equivalent) sidewall shape with the total (average) dose fixed.

$\mu C/cm^2$ (Distribution-A), the sidewall shape obtained is of overcut as can be seen in Figure 4.8(a), which is significantly different from the target one. The sidewall shape obtained with spatial dose control (Distribution-B), shown in Figure 4.8(b), is much closer to the target sidewall shape. With a constant dose, developing rates in edge regions of the line are smaller than those at the center region, so the resist in edge regions is developed slower vertically, leading to an overcut. When the dose is higher in edge regions of the line than in the center region as in the Distribution-B, the developing rate is higher in edge regions which causes lateral development at lower layers to start earlier. And also the exposure in

Dose Distribution	Average Dose ($\mu C/cm^2$)	Developing Time (sec)	Resist Profile (nm) Line Width		
			px_1	px_5	px_{10}
A:Dashed curve	640.0	40.0	130.0	130.0	129.0
B:Solid curve	560.0	40.0	131.6	131.0	129.0
C:Dotted curve	610.0	40.0	134.8	134.0	128.0

Table 4.3: The total (average) dose required to achieve the same (equivalent) sidewall shape with the developing time fixed.

unexposed regions tends to increase with depth. Therefore, lateral development following vertical development in the edge region catches up with vertical development right outside the edge region, leading to a more vertical sidewall shape. However, if the edge dose is increased beyond a certain level (with the average dose fixed) as in the Distribution-C, the effective developing rate is decreased significantly. This is due to the fact that the edge developing rate is much higher than that in its surrounding regime. Hence, the sidewall shape becomes overcut as seen in Figure 4.8(c).

The same set of the results for the average dose of 525 $\mu C/cm^2$ are provided in Figure 4.9. The sidewall for the increased constant dose, in Figure 4.9(a), is more vertical than that in Figure 4.8(a), but still not so vertical as that in Figure 4.8(b). As in the case of the average dose of 525 $\mu C/cm^2$, the spatial dose control with a small dose difference between the edge and center regions results in a much more vertical sidewall as can be seen in Figure 4.9(b), which is almost the same as that in Figure 4.8(b). Again, too large a dose difference between the edge and center regions leads to an overcut shown in Figure 4.9(c).

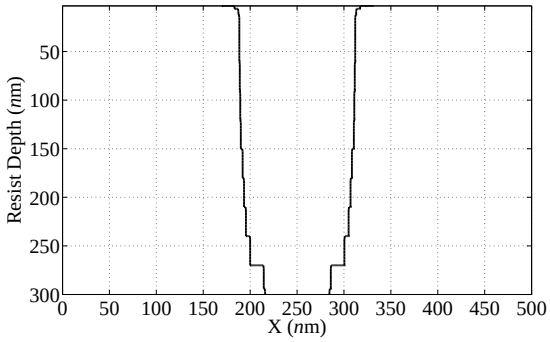

(a)

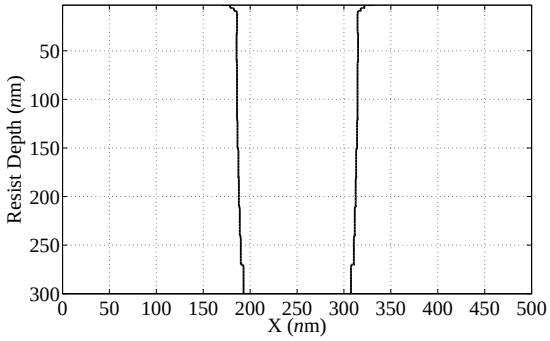

(b)

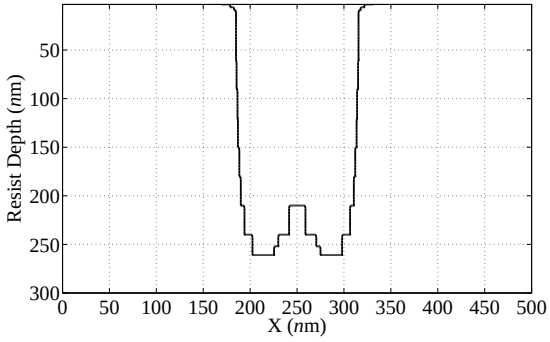

(c)

Figure 4.8: Simulation results with the same average dose 500 $\mu C/cm^2$ (a) simulation result for *Distribution-A* (b) simulation result for *Distribution-B* (c) simulation result for *Distribution-C* where developing time: 40 *sec*, MIBK:IPA=1:2, 300 nm PMMA on Si (50 KeV).

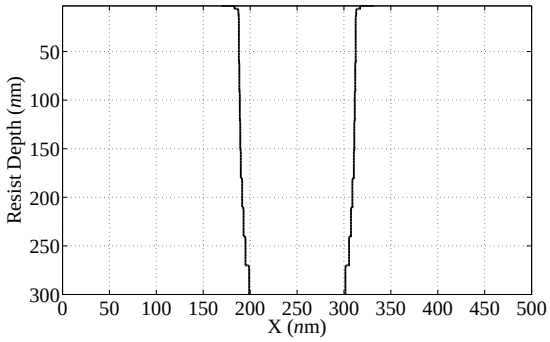

(a)

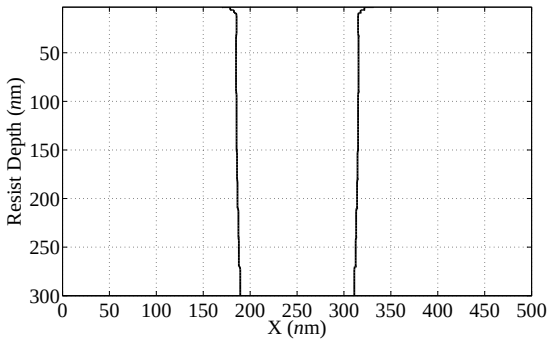

(b)

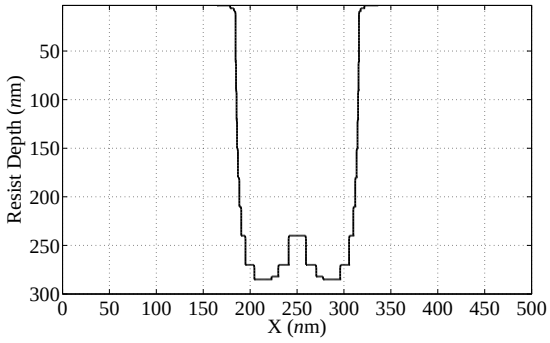

(c)

Figure 4.9: Simulation results with the same average dose 525 $\mu C/cm^2$ (a) simulation result for *Distribution-A* (b) simulation result for *Distribution-B* (c) simulation result for *Distribution-C* where developing time: 40 *sec*, MIBK:IPA=1:2, 300 nm PMMA on Si (50 KeV).

4.4 Trend Analysis of Sidewall Control

In this section, the relationship among dose distribution, developing time, average dose, resist thickness and the sidewall shape is analyzed through computer simulation. A line is partitioned into 5 regions along the length dimension and the dose distribution over the 5 regions is symmetric. Therefore, in the result tables, only the doses of 3 regions are provided (d_1, d_2, and d_3 are the doses of the edge, middle and center regions, respectively).

4.4.1 The Effect of Developing Time on Dose Distribution

For the same average dose and thickness, the developing time affects the dose distribution within the line, required to achieve the same sidewall shape of resist profile. As shown in Table 4.4, for 300 nm PMMA on Si , to achieve the equivalent sidewall shape with the average dose fixed, the dose difference between edge and center regions becomes smaller for a longer developing time. In general, the edge dose d_1 decreases while the center dose d_3 tends to increase with the increase of developing time. In addition, different combinations (small average dose/longer developing time or shorter developing time/larger average dose) can give the same resist profile.

Average Dose ($\mu C/cm^2$)	Developing Time (sec)	Dose Distribution			Target Profile (nm) Line Width			Actual Profile (nm) Line Width		
		d_1	d_2	d_3	rx_1	rx_5	rx_{10}	px_1	px_5	px_{10}
540.0	42.0	702.49	575.19	144.65	130.0	130.0	130.0	130.7	130.0	127.0
	44.0	701.85	518.10	260.09	130.0	130.0	130.0	131.6	131.0	129.0
	46.0	676.45	486.47	374.16	130.0	130.0	130.0	131.6	131.0	129.0
560.0	40.0	748.64	583.04	136.64	130.0	130.0	130.0	131.6	131.0	129.0
	42.0	687.84	631.19	161.94	130.0	130.0	130.0	130.7	131.0	130.0
	44.0	668.40	573.80	315.60	130.0	130.0	130.0	130.7	131.0	129.0
580.0	38.0	752.28	594.93	205.58	130.0	130.0	130.0	130.7	131.0	129.0
	40.0	691.11	673.72	170.34	130.0	130.0	130.0	130.7	130.0	130.0
	42.0	666.78	648.40	269.65	130.0	130.0	130.0	130.7	130.0	130.0
600.0	36.0	753.61	654.57	183.65	130.0	130.0	130.0	130.7	130.0	130.0
	38.0	717.63	651.94	260.86	130.0	130.0	130.0	130.7	130.0	130.0
	40.0	688.03	637.71	348.52	130.0	130.0	130.0	130.7	130.0	127.0

Table 4.4: Comparison of dose distributions with the same target resist profile (vertical sidewall) for line width of 100 nm and the same average dose (resist thickness: 300 nm).

For the resist thicknesses of 100 nm and 500 nm, the above trends still hold, as shown in Tables 4.5 and 4.6. For a thinner resist, it is easier to get vertical sidewalls and, from Table 4.5, it is seen that the slightly undercut sidewall can also be achieved. While for a thicker resist, it is imperative to increase the average dose significantly to fully develop it; the actual resist profile is far from the target profile. That is, it is more difficult to control the sidewall shape of a thicker resist. Note that the exposure varies more along the depth dimension when the resist is thicker.

Average Dose ($\mu C/cm^2$)	Developing Time (sec)	Dose Distribution			Target Profile (nm) Line Width			Actual Profile (nm) Line Width		
		d_1	d_2	d_3	rx_1	rx_5	rx_{10}	px_1	px_5	px_{10}
400.0	42.0	506.21	376.48	234.62	120.0	120.0	120.0	115.9	117.0	117.0
	44.0	485.31	373.88	281.63	120.0	120.0	120.0	115.9	117.0	117.0
	46.0	451.63	377.07	342.61	120.0	120.0	120.0	115.9	117.0	117.0
420.0	40.0	552.57	374.78	245.31	120.0	120.0	120.0	116.6	117.0	117.0
	42.0	496.28	439.09	229.25	120.0	120.0	120.0	115.9	117.0	117.0
	44.0	474.12	394.71	362.33	120.0	120.0	120.0	115.9	117.0	117.0
440.0	38.0	585.87	423.63	181.01	120.0	120.0	120.0	116.8	117.0	118.0
	40.0	516.53	437.32	292.30	120.0	120.0	120.0	115.9	117.0	118.0
	42.0	487.20	448.86	327.88	120.0	120.0	120.0	115.9	117.0	117.0

Table 4.5: Comparison of dose distributions with the same target resist profile (vertical sidewall) for line width of 100 nm and the same average dose (resist thickness: 100 nm).

Average Dose ($\mu C/cm^2$)	Developing Time (sec)	Dose Distribution			Target Profile (nm) Line Width			Actual Profile (nm) Line Width		
		d_1	d_2	d_3	rx_1	rx_5	rx_{10}	px_1	px_5	px_{10}
630.0	42.0	786.41	721.83	133.53	130.0	130.0	130.0	124.2	131.0	129.0
	44.0	737.85	734.31	205.67	130.0	130.0	130.0	124.2	131.0	130.0
	46.0	712.81	711.03	302.33	130.0	130.0	130.0	125.2	131.0	129.0
650.0	40.0	807.06	723.35	189.17	130.0	130.0	130.0	124.2	131.0	130.0
	42.0	775.89	666.32	365.57	130.0	130.0	130.0	124.2	131.0	129.0
	44.0	733.35	710.53	362.24	130.0	130.0	130.0	125.2	131.0	130.0
670.0	38.0	827.34	734.13	227.06	130.0	130.0	130.0	124.2	131.0	131.0
	40.0	779.76	733.90	322.67	130.0	130.0	130.0	124.2	131.0	131.0
	42.0	761.60	709.12	408.56	130.0	130.0	130.0	124.2	131.0	131.0

Table 4.6: Comparison of dose distributions with the same target resist profile (vertical sidewall) for line width of 100 nm and the same average dose (resist thickness: 500 nm).

From Tables 4.4-4.6, the effect of developing time on dose distribution is analyzed for the vertical sidewall shape. Given a target undercut sidewall shape, as shown in Table 4.7, a longer developing time results in a smaller dose difference between edge and center regions with the average dose and resist thickness (300 nm) fixed. Compared with the developing time required for a vertical sidewall in Table 4.4, a relatively longer developing time is desired in order to achieve an undercut sidewall for the same resist thickness.

Average Dose ($\mu C/cm^2$)	Developing Time (sec)	Dose Distribution			Target Profile (nm) Line Width			Actual Profile (nm) Line Width		
		d_1	d_2	d_3	rx_1	rx_5	rx_{10}	px_1	px_5	px_{10}
580.0	50.0	750.56	617.48	163.92	130.0	135.0	140.0	134.0	136.0	139.0
	52.0	740.07	545.74	328.40	130.0	135.0	140.0	134.0	136.0	139.0
	54.0	717.00	492.97	480.07	130.0	135.0	140.0	134.0	136.0	139.0
600.0	48.0	744.14	675.88	159.96	130.0	135.0	140.0	134.0	136.0	139.0
	50.0	736.32	624.25	278.85	130.0	135.0	140.0	134.0	136.0	139.0
	52.0	725.49	530.58	487.84	130.0	135.0	140.0	134.0	136.0	139.0
620.0	46.0	788.23	678.80	165.94	130.0	135.0	140.0	134.0	136.0	140.0
	48.0	735.57	703.73	221.40	130.0	135.0	140.0	134.0	136.0	140.0
	50.0	730.94	623.08	391.97	130.0	135.0	140.0	134.0	136.0	140.0

Table 4.7: Comparison of dose distributions with the same target resist profile (undercut sidewall) for line width of 100 nm and the same average dose (resist thickness: 300 nm).

4.4.2 The Effect of Average Dose on Dose Distribution

The average dose affects the spatial distribution of doses with the target profile and developing time fixed. The dose difference between edge and center regions becomes smaller for a larger average dose, which can be seen from Tables 4.8-4.11. That is, the dose distribution becomes flatter as the average dose increases. Therefore, one of the ways to achieve a vertical sidewall or undercut sidewall is to increase the dose level of uniform distribution, which however requires a longer exposing time and leads to a larger charging effect.

Developing Time (sec)	Average Dose ($\mu C/cm^2$)	Dose Distribution			Target Profile (nm) Line Width			Actual Profile (nm) Line Width		
		d_1	d_2	d_3	rx_1	rx_5	rx_{10}	px_1	px_5	px_{10}
38.0	580.0	752.28	594.93	205.58	130.0	130.0	130.0	130.7	131.0	129.0
	600.0	717.63	651.94	260.86	130.0	130.0	130.0	130.7	130.0	130.0
	620.0	699.56	678.02	344.83	130.0	130.0	130.0	130.7	130.0	130.0
40.0	560.0	748.64	583.04	136.64	130.0	130.0	130.0	131.6	131.0	129.0
	580.0	691.11	673.72	170.34	130.0	130.0	130.0	130.7	130.0	130.0
	600.0	688.03	637.71	348.52	130.0	130.0	130.0	130.7	130.0	127.0
42.0	540.0	702.49	575.19	144.65	130.0	130.0	130.0	130.7	130.0	127.0
	560.0	687.84	631.19	161.94	130.0	130.0	130.0	130.7	131.0	130.0
	580.0	666.78	648.40	269.65	130.0	130.0	130.0	130.7	130.0	130.0

Table 4.8: Comparison of dose distributions with the same target resist profile (vertical sidewall) for line width of 100 nm and the same developing time (resist thickness: 300 nm).

Developing Time (sec)	Average Dose ($\mu C/cm^2$)	Dose Distribution			Target Profile (nm) Line Width			Actual Profile (nm) Line Width		
		d_1	d_2	d_3	rx_1	rx_5	rx_{10}	px_1	px_5	px_{10}
40.0	420.0	552.57	374.78	245.31	120.0	120.0	120.0	116.6	117.0	117.0
	440.0	516.53	437.32	292.30	120.0	120.0	120.0	115.9	117.0	118.0
	460.0	493.25	474.07	365.37	120.0	120.0	120.0	115.9	117.0	117.0
42.0	400.0	506.21	376.48	234.62	120.0	120.0	120.0	115.9	117.0	117.0
	420.0	496.28	439.09	229.25	120.0	120.0	120.0	115.9	117.0	117.0
	440.0	487.20	448.86	327.88	120.0	120.0	120.0	115.9	117.0	117.0
44.0	380.0	491.50	323.89	269.23	120.0	120.0	120.0	115.9	116.0	116.0
	400.0	485.31	373.88	281.63	120.0	120.0	120.0	115.9	117.0	117.0
	420.0	474.12	394.71	362.33	120.0	120.0	120.0	115.9	117.0	117.0

Table 4.9: Comparison of dose distributions with the same target resist profile (vertical sidewall) for line width of 100 nm and the same developing time (resist thickness: 100 nm).

Developing Time (sec)	Average Dose ($\mu C/cm^2$)	Dose Distribution			Target Profile (nm) Line Width			Actual Profile (nm) Line Width		
		d_1	d_2	d_3	rx_1	rx_5	rx_{10}	px_1	px_5	px_{10}
40.0	650.0	807.06	723.35	189.17	130.0	130.0	130.0	124.2	131.0	130.0
	670.0	779.76	733.90	322.67	130.0	130.0	130.0	124.2	131.0	131.0
	690.0	775.97	673.47	551.12	130.0	130.0	130.0	124.2	131.0	129.0
42.0	630.0	786.41	721.83	133.53	130.0	130.0	130.0	124.2	131.0	129.0
	650.0	775.89	666.32	365.57	130.0	130.0	130.0	124.2	131.0	129.0
	670.0	761.60	709.12	408.56	130.0	130.0	130.0	124.2	131.0	131.0
44.0	610.0	745.71	726.24	106.09	130.0	130.0	130.0	124.2	131.0	128.0
	630.0	737.85	734.31	205.67	130.0	130.0	130.0	124.2	131.0	130.0
	650.0	733.35	710.53	362.24	130.0	130.0	130.0	125.2	131.0	130.0

Table 4.10: Comparison of dose distributions with the same target resist profile (vertical sidewall) for line width of 100 nm and the same developing time (resist thickness: 500 nm).

4.4.3 The Effect of Developing Time on Sidewall Shape

The developing time has a significant effect on the sidewall shape of a line. In general, a longer developing time results in a more vertical or undercut sidewall for a given dose distribution, as shown in Tables 4.12 and 4.13. The dose distributions in Tables 4.12 and 4.13 are derived from the SA method with the target profile: $rx_1 = 130n$m, $rx_5 = 130n$m, $rx_{10} = 130n$m and the developing time: 40.0 *sec*. Based on these dose distributions, the developing time is varied to see its effect on the sidewall shape. A longer developing time allows a longer time for lateral development. And the developing rate in the unexposed region increases with depth, therefore, the lateral development following vertical development in the unexposed region catches up with vertical development right outside the edge region, resulting in a more vertical sidewall shape and eventually an undercut.

4.4.4 The Effect of Dose Distribution on Sidewall Shape

In Table 4.14, the dose distributions which minimize the deviation from the target sidewall shape and were obtained by the SA method are listed. For each thickness of resist, the combination of the developing time and minimum average dose is varied. In order to quantify the characteristic of dose distribution, d_1, d_2 and d_3 normalized by d_1 are also included in the table. It is observed that d_2 becomes closer to d_1 with d_1 still greater than d_2

Developing Time (sec)	Average Dose ($\mu C/cm^2$)	Dose Distribution			Target Profile (nm) Line Width			Actual Profile (nm) Line Width		
		d_1	d_2	d_3	rx_1	rx_5	rx_{10}	px_1	px_5	px_{10}
48.0	600.0	744.14	675.88	159.96	130.0	135.0	140.0	134.0	136.0	139.0
	620.0	735.57	703.73	221.40	130.0	135.0	140.0	134.0	136.0	140.0
	640.0	728.29	665.42	412.58	130.0	135.0	140.0	134.0	136.0	140.0
50.0	580.0	750.56	617.48	163.92	130.0	135.0	140.0	134.0	136.0	139.0
	600.0	736.32	624.25	278.85	130.0	135.0	140.0	134.0	136.0	139.0
	620.0	730.94	623.08	391.97	130.0	135.0	140.0	134.0	136.0	140.0
52.0	560.0	780.71	530.60	177.39	130.0	135.0	140.0	135.0	136.0	138.0
	580.0	740.07	545.74	328.40	130.0	135.0	140.0	134.0	136.0	139.0
	600.0	725.49	530.58	487.84	130.0	135.0	140.0	134.0	136.0	139.0

Table 4.11: Comparison of dose distributions with the same target resist profile (undercut sidewall) for line width of 100 nm and the same developing time (resist thickness: 300 nm).

Developing Time (sec)	Dose Distribution			Actual Profile (nm) Line Width		
	d_1	d_2	d_3	px_1	px_5	px_{10}
40.0	748.64	583.04	136.64	131.6	131.0	129.0
46.0	748.64	583.04	136.64	132.6	133.0	133.0
48.0	748.64	583.04	136.64	133.8	134.0	135.0
60.0	748.64	583.04	136.64	136.0	139.0	143.0

Table 4.12: The effect of developing time on sidewall shape with the average dose (560.0 $\mu C/cm^2$) and dose distribution fixed (resist thickness: 300 nm).

as the resist thickness increases. Also, d_3 is relatively smaller for a thicker resist. In addition, it can be seen that the normalized d_1, d_2 and d_3 remain similar within each thickness of resist.

Developing Time (sec)	Dose Distribution			Actual Profile (nm) Line Width		
	d_1	d_2	d_3	px_1	px_5	px_{10}
40.0	807.06	723.35	189.17	124.2	131.0	130.0
42.0	807.06	723.35	189.17	124.2	132.0	133.0
48.0	807.06	723.35	189.17	126.0	135.0	141.0
60.0	807.06	723.35	189.17	129.6	141.0	152.0

Table 4.13: The effect of developing time on sidewall shape with the average dose (650.0 $\mu C/cm^2$) and dose distribution fixed (resist thickness: 500 nm).

Resist Thickness (nm)	Average dose ($\mu C/cm^2$)	Developing time (sec)	Dose Distribution			Ratio	Target Profile (nm) Line Width			Actual Profile (nm) Line Width		
			d_1	d_2	d_3	$\frac{d_1}{d_1} : \frac{d_2}{d_1} : \frac{d_3}{d_1}$	rx_1	rx_5	rx_{10}	px_1	px_5	px_{10}
100	400.0	42.0	506.2	376.5	234.6	1:0.744:0.464	120.0	120.0	120.0	115.9	117.0	117.0
	420.0	40.0	552.6	374.8	245.3	1:0.678:0.444	120.0	120.0	120.0	116.6	117.0	117.0
	440.0	38.0	585.9	423.6	181.0	1:0.723:0.309	120.0	120.0	120.0	116.8	117.0	118.0
300	540.0	42.0	702.5	575.2	144.7	1:0.819:0.206	130.0	130.0	130.0	130.7	130.0	127.0
	560.0	40.0	748.6	583.0	136.6	1:0.779:0.183	130.0	130.0	130.0	131.6	131.0	129.0
	580.0	38.0	752.3	594.9	205.6	1:0.791:0.273	130.0	130.0	130.0	130.7	131.0	129.0
500	630.0	42.0	786.4	721.8	133.5	1:0.918:0.170	130.0	130.0	130.0	124.2	131.0	129.0
	650.0	40.0	807.1	723.4	189.2	1:0.896:0.234	130.0	130.0	130.0	124.2	131.0	130.0
	670.0	38.0	827.3	734.1	227.1	1:0.887:0.274	130.0	130.0	130.0	124.2	131.0	131.0

Table 4.14: Comparison of dose distributions required to achieve a target sidewall shape for different resist thicknesses. For each given developing time, the average dose is minimized.

Chapter 5

Concluding Remarks and Future Study

In this thesis, the related problems of step-width adjustment and sidewall control in electron-beam lithography have been studied, based on the common framework of 3-D exposure model and resist development simulation.

Due to lateral development of step sidewalls in a staircase structure during the resist development process, the step-widths in the final resist profile may be substantially different from the target widths. A practical method for adjusting step-widths, developed for staircase structures, is described. The method is based on a 3-D exposure model and utilizes the exposure-to-rate conversion formula derived from experimental results. The method estimates step-width deviation and then compensates for the deviation by a combination of width adjustment and dose control, which achieves a fine control of step-width and height. Also, the issue of sidewall control has been further investigated based on the results from the previous work. A line is partitioned into regions along the length dimension and a dose is determined for each region. It is attempted to find the optimum dose distribution by the general-purpose optimization scheme, Simulated Annealing. Through computer simulation, the effects of the factors such as dose distribution, total dose and developing time, and performance of the dose control scheme have been analyzed. The future research efforts include application of the proposed methods to more general structures and multiple lines, and experimental verification.

Bibliography

[1] Ampere A. Tseng, Kuan Chen, Chii D. Chen, and Kung J. Ma, "Electron beam lithography in nanoscale fabrication: recent development," *IEEE Transactions on Electronics Packaging Manufacturing* vol. 26, no. 2, pp. 141-149, April 2003.

[2] W. Hu, K. Sarveswaran, M. Lieberman and G. H. Bernstein, "High-resolution electron beam lithography and DNA nano-patterning for molecular QCA," *IEEE Transactions on In Nanotechnology*, vol. 4(3), pp. 312-316, 2005.

[3] H. Kawano, H. Ito, K. Mizuno, T. Matsuzaka, K. Kawasaki, N. Saitou, H. Ohta, and Y. Sohda, "Development of an electron-beam lithography system for high accuracy masks," *Journal of Vacuum Science and Technology*, B 21(2), pp. 823-827, Mar. 2003.

[4] S. Y. Chou *et al.*, "Sub-10 nm imprint lithography and applications," *Journal of Vacuum Science and Technology*, B 15(6), pp. 2897-2904, Nov./Dec. 1997.

[5] T. H. P. Chang, "Proximity effect in electron-beam lithography," *Journal of Vacuum Science and Technology*, 12(6), pp. 1271-1275, Nov./Dec. 1975.

[6] Sherry J. Gillespie, "Resist profile control in e-beam lithography", *IBM J. Res. Develop.*, pp. 454-460, July 1984.

[7] Y. C. Patil, A. Teolis, D. Park, R. Bass, K. Rhee, B. Bradie, M. C. Peckerar, "An error measure for dose correction in e-beam nanolithography", *Journal of Vacuum Science and Technology*, B 8(6), Nov./Dec. 1990.

[8] V. V. Aristov, B. N. Gaifullin, A. A. Svinstov, S. I. Zaitsev, H. F. Raith, R. Jede, "Accuracy of proximity effect correction in electron lithography after development", *Journal of Vacuum Science and Technology*, B 10(6), Nov./Dec. 1992.

[9] Jianyun Zhou, Xiaomin Yang, "Monte Carlo simulation of process parameters in electron beam lithography for thick resist patterning", *Journal of Vacuum Science and Technology*, B 24(3), May/June 2006.

[10] M. Parikh, "Correction to proximity effects in electron-beam lithography. II. Implementation", *Journal of Applied Physics*, vol. 50, no. 6, pp. 4371-4382, June 1979.

[11] N. D. Wittels and C. Youngman, "Proximity effect correction in electron-beam lithography", *Proceedings of the 8th International Conference on Electron and Ion Beam Science and Technology*, ed. by R. Bakish, Electrochemical Society, Princeton, New York, pp. 361-365, 1978.

[12] D. P. Kern, "A Novel Approach to Proximity Effect Correction", *Proceedings of the 9th International Conference on Electron and Ion Beam Science and Technology*, ed. by R. Bakish, Electrochemical Society, Princeton, New York, pp. 326-339, 1980.

[13] D. Chow, J. McDonald, C. King, W. Smith and A. J. Steckl, "An image processing approach to fast, efficient proximity effect correction for electron-beam lithography", *Journal of Vacuum Science and Technology*, vol. 1, pp. 1383-1390, Oct./Dec. 1983.

[14] J. Greeneich, "Proximity effect correction using a dose compensation curve", *Journal of Vacuum Science and Technology*, vol. 19, pp. 1269-1274, Nov./Dec. 1983.

[15] M. Parikh, "Calculation of changes in pattern dimensions to compensate for proximity effects in electron-beam lithography", *Journal of Applied Physics*, vol. 51, pp. 705-709, January 1980.

[16] M. Parikh, "Correction to proximity effects in electron-beam lithography. III. Experiments", *Journal of Applied Physics*, vol. 50, no. 6, pp. 4383-4387, June 1979.

[17] M. Parikh, "Proximity Effect Corrections in Electron Beam Lithography", *Proceedings of the 8th International Conference on Electron and Ion Beam Science and Technology*, ed. by R. Bakish, Electrochemical Society, Princeton, New York, pp. 382-391, 1978.

[18] S.K.S. Ma, M. Parikh, and W. Ward, "Proximity Corrections in a Raster Scan Electron Lithography Machine", *Journal of Vacuum Science and Technology*, vol. 19, no. 4, pp. 1275-1278, Nov./Dec. 1981.

[19] W. T. Lynch, T. E. Smith, W. Fichtner, "An algorithm for proximity effect correction with E beam exposure", *International Conference on Microlithography*, Microcircuit Engineering, pp. 309-314, Oct. 5-8, 1982.

[20] G. Owen, "Methods for proximity effect correction in electron-beam lithography", *Journal of Vacuum Science and Technology*, vol. 8, pp. 1889-1892, Nov./Dec. 1990.

[21] S.-Y. Lee, J.C. Jacob, C.M. Chen, J.A. McMillan, and N.C. MacDonald, "Proximity effect correction in electron-beam lithography: A hierarchical, rule-based scheme-PYRAMID", *Journal of Vacuum Science and Technology*, vol. B9, pp. 3048-3053, Nov./Dec. 1991.

[22] J.C. Jacob, S.-Y. Lee, J.A. McMillan, and N.C. MacDonald, "Fast proximity effect correction: An extension of PYRAMID for circuit patterns of arbitrary size", *Journal of Vacuum Science and Technology*, vol. B10, pp. 3077-3082, Nov./Dec. 1992.

[23] J.C. Jacob, "PYRAMID - A hierarchical, rule-based scheme for proximity effect correction in electron-beam lithography: An Implementation for single layer circuits", *Masters Thesis*, Cornell University, 1992.

[24] S.-Y. Lee and B. D. Cook, "PYRAMID-A Hierarchical, Rule-Based Approach Toward Proximity Effect Correction-Part I: Exposure Estimation," *IEEE Transactions on Semiconductor Manufacture*, vol. 11, no. 1, pp. 108-116, Feb. 1998.

[25] B. D. Cook and S.-Y. Lee, "PYRAMID-A Hierarchical, Rule-Based Approach Toward Proximity Effect Correction-Part II: Correction," *IEEE Transactions on Semiconductor Manufacture*, vol. 11, no. 1, pp. 117-127, Feb. 1998.

[26] B. D. Cook, "PYRAMID - A Hierarchical, Rule-Based Proximity Effect Correction Scheme for electron-beam lithography: Generalization and optimization for homogeneous substrates", *Ph.D. Dissertation*, Cornell University, August 1996.

[27] B. D. Cook and S.-Y. Lee, "Dose, shape and hybrid modifications for PYRAMID in electron beam proximity effect correction", *Journal of Vacuum Science and Technology*, B 15(6), pp. 2303-2308, Nov./Dec. 1997.

[28] B. D. Cook and S.-Y. Lee, "Fast Exposure Simulation for Large Circuit Patterns in Electron Beam Lithography", *Proceedings of the International Conference on Image Processing*, pp. 442-445, October 1995.

[29] B. D. Cook and S.-Y. Lee, "Performance Analysis and Optimal Parameter Selection for PYRAMID", *Proceedings of the International Conference on Mico- and Nano- Engineering*, pp. 61-64, September, 1995.

[30] S.-Y. Lee and B. D. Cook, "Interior Area Removal Method for PYRAMID", *Journal of Vacuum Science and Technology*, vol. B 12(6), pp. 3449-3454, Nov./Dec. 1994.

[31] B. D. Cook and S.-Y. Lee, "A Quantitative Performance Analysis of PYRAMID", *Proceedings of the International Conference on VLSI and CAD*, pp. 16-18, November, 1993.

[32] B. D. Cook and S.-Y. Lee, "Fast Proximity Effect Correction: An Extension of PYRAMID for Thicker Resists", *Journal of Vacuum Science and Technology*, vol. B 7(6), pp. 1556-1560, Nov./Dec. 1989.

[33] S.-Y. Lee, B. Liu, B. D. Cook, "Reducing recursive effect for fast proximity correction", *Microelectronic Engineering*, vol. 35, pp. 491-494, 1997.

[34] S.-Y. Lee and J. Laddha, "Adaptive selection of control points for improving accuracy and speed of proximity effect correction", *Journal of Vacuum Science and Technology*, vol. B 16(6), pp. 3269-3274, Nov./Dec. 1998.

[35] J. Laddha and S.-Y. Lee, "Application of neural network to enhancing accuracy of E-beam proximity effect correction", *Microelectronic Engineering*, no. 53, pp. 317-320, 2000.

[36] S.-Y. Lee and D. He, "Simultaneous dose modification for balanced e-beam proximity effect correction minimizing CD error", *Microelectronic Engineering*, no. 69, pp. 47-56, 2003.

[37] S.-Y. Lee and B. Liu, " Region-wise proximity effect correction for heterogeneous substrates in e-beam lithography:shape modification", *Journal of Vacuum Science and Technology*, B 14(6), pp. 3874-3879, Nov./Dec. 1996.

[38] F. Hu and S.-Y. Lee, "Dose control for fabrication of grayscale structures using a single step electron-beam lithographic process", *Journal of Vacuum Science and Technology*, B 21(6), pp. 2672-2679, Nov. 2003.

[39] S.-Y. Lee, F. Hu, and J. Ji, "Representation of non-rectangular features for exposure estimation and proximity effect correction in electron-beam lithography", *Journal of Vacuum Science and Technology*, B 22(6), pp. 2929-2935, Nov./Dec. 2004.

[40] S.-Y. Lee and K. Anbumony, "Analysis of three-dimensional proximity effect in electron-beam lithography," *Microelectronic Engineering*, vol. 83(2), pp. 336-344, Feb. 2006.

[41] S.-Y. Lee and K. Anbumony, "Accurate control of remaining resist depth for nanoscale three-dimensional structures in electron-beam grayscale lithography," *Journal of Vacuum Science and Technology*, B 25(6), pp. 2008-2012, Nov. 2007.

[42] K. Anbumony and S.-Y. Lee, "True three-dimensional proximity effect correction in electron-beam lithography," *Journal of Vacuum Science and Technology*, B 24(6), pp. 3115-3120, Nov./Dec. 2006.

[43] M. Gentili, L. Grella, A. Lucchesini, L. Luciani, L. Mastrogiacomo, and P. Musumeci, "Energy density function determination in very-high-resolution electron-beam lithography", *Journal of Vacuum Science and Technology*, B 8(6), pp. 1867-1871, Nov./Dec. 1990.

[44] M. Osawa, T. Yao, H. Aoyama, K. Ogino, H. Hoshino, Y. Machida, S. Asai, and H. Arimoto, "Correction for local flare effects approximated with double Gaussian profile in ArF lithography", *Journal of Vacuum Science and Technology*, B 21(6), pp. 2806-2809, Nov./Dec. 2003.

[45] J. Kim, D. C. Joy and S.-Y. Lee, "Controlling resist thickness and etch depth for fabrication of 3D structures in electron-beam grayscale lithography," *Microelectronic Engineering*, vol. 84(12), pp. 2859-2864, Dec. 2006.

[46] D. Kyser and N. Viswanathan, "Monte Carlo simulation of spatially distributed beams in electron-beam lithography," *Journal of Vacuum Science and Technology*, vol. 12(6), pp. 1305-1308, Nov. 1975.

[47] Y. Hirai, S. Tomida, K. Ikeda, M. Sasago, M. Endo, S. Hayama, and N. Nomura, "Three-dimensional resist process simulator PEACE (Photo and electron beam lithography analyzing computer engineering system)," *IEEE Transactions on Computer-Aided Design* vol. 10, pp. 802-807, June 1991.

[48] P. Li and S.-Y. Lee, "Step-width adjustment in fabrication of staircase structures," *Journal of Vacuum Science and Technology*, B 28(1), pp. 30-35 Jan. 2010.

[49] W. Goffe, G. Ferrier, and J. Rogers, "Global optimization of statistical functions with simulated annealing," *Journal of Econometrics*, vol. 60, pp. 65-99, Jan./Feb. 1994.